KfK 5256
Dezember 1993

Fracture Mechanical Treatment of Bridging Stresses in Ceramics

T. Fett, D. Munz
Institut für Materialforschung

Kernforschungszentrum Karlsruhe

KERNFORSCHUNGSZENTRUM KARLSRUHE
Institut für Materialforschung

KfK 5256

Fracture mechanical treatment of bridging stresses in ceramics

T. Fett, D. Munz

Kernforschungszentrum Karlsruhe GmbH, Karlsruhe

Als Manuskript gedruckt

Kernforschungszentrum Karlsruhe GmbH
Postfach 3640, 76021 Karlsruhe

ISSN 0303-4003

Fracture mechanical treatment of bridging stresses in ceramics

Abstract

Failure of ceramic materials often starts from cracks which can originate at pores, inclusions or can be generated during surface treatment. Fracture occurs when the stress intensity factor of the most serious crack in a component reaches a critical value K_{Ic}, the fracture toughness of the material. In case of ideal brittle materials the fracture toughness is independent of the crack extension and, consequently, identical with the stress intensity factor K_{I0} necessary for the onset of stable crack growth.
It is a well-known fact that failure of several ceramics is influenced by an increasing crack-growth resistance curve. Several effects are responsible for this behaviour: Crack-border interactions in the wake of the advancing crack, residual stress fields in the crack region of transformation-toughened ceramics, the generation of a micro-crack zone ahead the crack tip and crack branching.
The effect of increasing crack resistance has consequences on many properties of ceramic materials. In this report the authors discuss the some aspects of R-curve behaviour as the representation by stress intensity factors or energies and the influence on the compliance using the bridging stress model.

Bruchmechanische Behandlung von Brückenspannungen in Keramiken

Kurzfassung

Das Versagen keramischer Werkstoffe geht häufig von Rissen aus, die an Poren und Einschlüssen entstehen oder bei der Oberflächenbearbeitung verursacht werden.
Versagen einer keramischen Komponente tritt dann auf, wenn für den gefährlichsten Riß der kritische Spannungsintensitätsfaktor K_{Ic} erreicht wird. Im Falle ideal spröder Materialien ist die Rißzähigkeit K_{Ic} unabhängig von der Rißverlängerung und damit stets gleich dem zur Einleitung der Rißverlängerung notwendigen spezifischen Spannungsintensitätsfaktor K_{I0}. Es gibt nun eine Reihe von Keramiken bei denen der Rißwiderstand mit zunehmender Rißverlängerung anwächst.
Mehrere Effekte können für diese Erscheinung verantwortlich gemacht werden: Rißflankenverhakungen im Bereich hinter der Rißspitze, Spannungsfelder im Rißspitzenbereich aufgrund von Phasenumwandlungen in umwandlungsverstärkten Keramiken, die Entwicklung einer Mikrorißzone im Rißspitzenbereich sowie der Effekt der Rißverzweigung. Der Anstieg des Rißwiderstands hat Konsequenzen auf eine Reihe von Eigenschaften der Keramiken. In dieser Arbeit soll über die Darstellung der R-Kurven in Form von Spannungsintensitätsfaktoren sowie der Energiefreisetzungsrate und über den Einfluß der R-Kurve auf die Probennachgiebigkeit berichtet werden.

Contents

1.0 Introduction 1

2.0 Basic relations 3

3.0 Energy considerations 7

3.1 Definition of the crack driving force 7
3.1.1 Linear-elastic material behaviour 7
3.1.2 Nonlinear-elastic material behaviour 8
3.1.3 Stress intensity factors, J-integral and energy release rate 10
3.1.4 Special assumption on bridging stresses 11

3.2 The crack resistance 12
3.2.1 Energy balance during crack propagation 12
3.2.2 The crack resistance and the applied stress intensity factor 16

3.3 Application of a Dugdale model by Evans and McMeeking 17

3.4 R-curve for a Griffith crack with constant bridging stresses 19

3.5 Conclusions 23

4.0 Compliance and R-curve 25

4.1 Compliance 25
4.1.1 Loading-point compliance 25
4.1.2 Crack-mouth compliance 30

4.2 R-curves 31
4.2.1 Calculation of R-curves 31
4.2.2 Experimental R-curves 31

5.0 References 39

Appendix A. 41

A.1 Bridging relations for numerical calculations 41
A.1.1 Bridging stresses based on friction effects 41
A.1.2 Springs with limited extensions 42

A.2 Derivation of eq.(2.2) 45

A.3 Derivation of eq.(2.4) 46

A.4 Relations for bending load 47

1.0 Introduction

Several ceramic materials show R-curve effects, i.e. an increase in crack-growth resistance with increasing crack depth. Different effects are responsible for this behaviour. In coarse-grained alumina the crack growth resistance increases with increasing crack extension due to friction-like crack-border interactions in the wake of the advancing crack. The correlated "bridging stresses" are extremely non-linear and their range of extension is not negligible compared with the crack length. The consequences of the bridging interactions on fracture-mechanical considerations may become very serious. Some special questions are:

- What is the meaning of the compliance in presence of non-linear bridging interactions?
- Is crack-length measurement by means of compliance correct?
- Does the Irwin formula between the energy release rate G_I or the J-integral and the stress intensity factor K_I

$$J = G = K_I^2/E' \tag{1.1}$$

  with $E' = E/(1 - \nu^2)$, E = Young's modulus, and ν = Poisson ratio, also hold in the presence of an R-curve effect?
- Is the crack growth resistance R related to the applied stress intensity factor $K_{I\,appl}$ by the simple relation

$$R = K_{I\,appl}^2/E' \tag{1.2}$$

  as usual in linear-elastic fracture mechanics?

The consequences of specially chosen bridging-stress relations were studied in the literature. In this investigation the questions mentioned before will be treated as much as possible analytically, and special bridging relations will be used only to illustrate the effects.

2.0 Basic relations

Let us consider a specimen (fig.1) of width W, thickness B, and length $2L$ which contains a crack of depth a_0 with completely separated crack surfaces (produced, e.g., by a very narrow saw-cut with negligible notch-root radius). Starting from this initial crack size, a crack may propagate under increasing external loads, and in case of coarse-grained materials bridging interactions occur which result in so-called bridging stresses depending on the actual crack opening displacements δ.

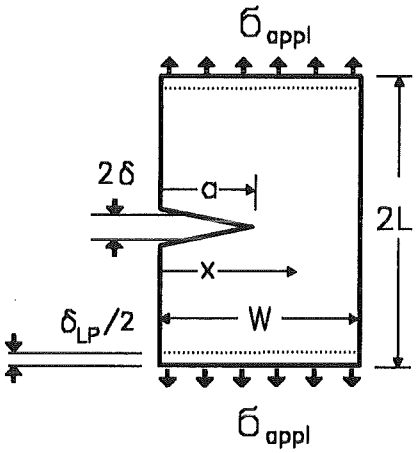

Figure 1. . Geometrical data of an edge-cracked plate under tensile load.

The externally applied load P is related to σ_{appl} by

$$P = \sigma_{appl} WB \tag{2.1}$$

where B is the thickness of the plate.
For the description of crack opening and crack propagation in terms of energy we consider a crack of total length a with crack surface interactions in the range $a_0 < x < a$ in the unloaded state ($\delta = 0$).
The specimen is exposed to increasing externally applied stresses σ_{appl} at the free ends of the specimen. For reasons of simplicity this stress is assumed to be constant, i.e. independent of the coordinate x. The crack-opening displacement field can be calculated by use of the fracture-mechanical weight-function method. This follows from two important relations ((2.2) and (2.3)).

Rice [1] has shown that the weight function can be derived from the crack opening displacements of any reference load case (subscript r) and the related reference stress intensity factor

$$h_I(x, a) = \frac{E'}{K_{Ir}} \frac{\partial}{\partial a} \delta_r(x, a) \tag{2.2}$$

with $E' = E/(1 - \nu^2)$ for plane strain, E = Young's modulus, and ν = Poisson's ratio. A simple derivation of this important relation is given in Appendix A.2. K_I is the mode-I stress intensity factor, which can be computed for the stress distribution σ_r in the uncracked component perpendicular to the crack using Bückner's relation [2]

$$K_{Ir} = \int_0^a \sigma_r(x)\, h(x,a)\, dx \tag{2.3}$$

The reference stress distribution can be any arbitrary stress distribution. Based on eqs.(2.2) and (2.3) the crack opening displacements result by integration [3]

$$\delta(x) = \frac{1}{E'} \int_0^a \int_{\max(x,x')}^a h(a',x)\, h(a', x')\, \sigma(x')\, da'dx' \tag{2.4}$$

where the index r in the stress is omitted. The detailed calculations are outlined in Appendix A.3. Equation (2.4) can also be derived from the equivalent procedure developed by Paris [4], [5] which is based on Castigliano's theorem. Equation (2.4) was also sucessfully applied by Cox and Marshall [6]. If a special stress relation is given, the solution of the integral equation (2.4) can be determined by successive approximation or other strategies which are well known in numerical mathematics.
In eq.(2.4) x is the coordinate where the displacement is computed and x' is the location where the stress σ acts. If the applied stress σ_{appl} as well as bridging stresses σ_{br} act on the crack surfaces, the total stress is

$$\sigma_{total} = \sigma_{appl} + \sigma_{br} \quad ; \quad \sigma_{br} < 0 \tag{2.5}$$

and the total crack opening displacements result as

$$\delta_{total}(x) = \delta_{appl} + \delta_{br} = \frac{1}{E'} \int_0^a \int_{\max(x,x')}^a h(a',x)\, h(a', x')\, [\sigma_{appl}(x') + \sigma_{br}(x')]\, da'dx' \tag{2.6}$$

where δ_{appl} is the displacement caused by the applied stress. $\sigma_{appl}(x')$ is the stress in the uncracked component at the location of the crack. For the plate under uniform tension $\sigma_{appl}(x)$ is identical with the externally applied stress. Note that δ_{total} is the crack opening displacement of one crack border, whereas δ_{LP} is the total load point displacement (see fig.2). As an example of application the integral equation (2.6) has been solved numerically for an exponential bridging relation as given by eqs.(A1) and (A3) in Appendix A.1. The displacements are plotted in fig.2. The displacements caused by the bridging stresses are negative, it should be noted that in fig.2 the absolute values are shown. Figure 3 represents the distribution of the bridging stresses.
Far away from the crack, the crack opening displacements δ_{total} lead to displacements δ_{LP} which will be called the "loading-point displacements". It holds for tensile loading

$$\delta_{LP} = \frac{\sigma_{appl}}{E} 2L + \frac{2}{W} \int_0^a \delta_{total}(x)\, dx \tag{2.7}$$

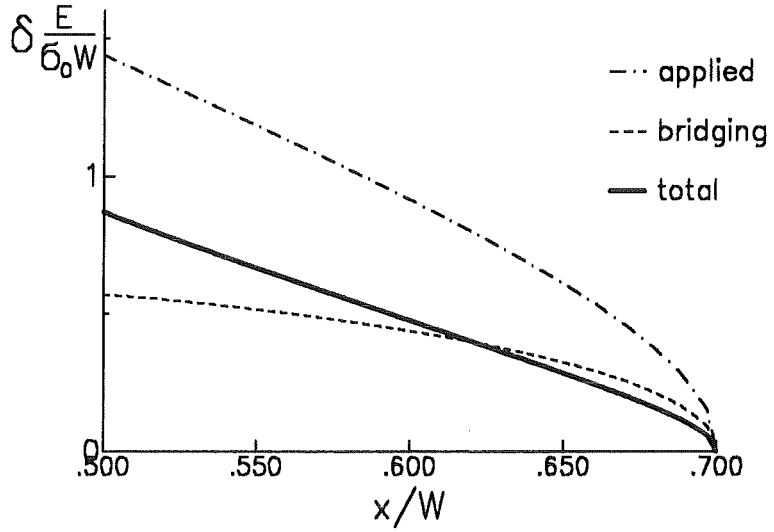

Figure 2. . Profile of the crack faces in the region of bridging interactions, computed with the bridging stress relation eq.(A1 + A3) for an applied tensile stress $\sigma_{appl}/\sigma_0 = 0.17$ and $a_0/W = 0.5$ (bridging displacements in absolute values).

A similar relation for bending is derived in Appendix A.4. The first term in (2.7) represents the displacements of the uncracked structure in pure tension and the second term is the contribution by the crack. If a minimum length of $L > W$ is ensured the stress intensity factor and δ_{total} are independent of L. In all further equations the first term in (2.7) is omitted.
Under loading conditions different from pure tension ($\sigma_{appl} \neq constant$) (2.7) has to be replaced by

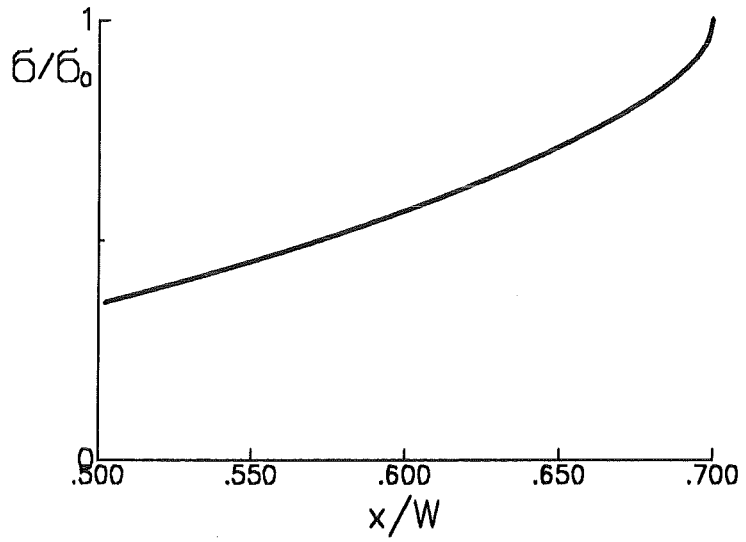

Figure 3. . Bridging-stress distribution computed with the bridging-stress relation eq.(A1 + A3) for an applied tensile stress $\sigma_{appl}/\sigma_0 = 0.17$, $a_0/W = 0.5$.

$$P\, d\delta_{LP} = +2B\int_0^a \sigma_{appl}\, d\delta_{total}(x)\, dx \tag{2.8}$$

The total stress intensity factor which is responsible for the stress state at the crack tip results by superposition of the applied stress intensity factor $K_{I\,appl}$ and the bridging stress intensity factor K_{Ibr} as

$$K_{total} = K_{I\,tip} = K_{I\,appl} + K_{Ibr} \quad ; \quad K_{Ibr} < 0 \tag{2.9}$$

with

$$K_{I\,appl} = \int_0^a \sigma_{appl}(x)\, h(x,a)\, dx \tag{2.3a}$$

$$K_{Ibr} = \int_0^a \sigma_{br}(x)\, h(x,a)\, dx \tag{2.3b}$$

The work W_{appl} due to the crack done by the stresses σ_{appl} during crack opening up to the displacements $\delta_{total}(x)$ is given by

$$W_{appl} = 2B\int_0^a dx \int_0^{\delta_{total}} \sigma'_{appl}\, d\delta'_{total} \tag{2.10}$$

where the prime denotes the integration variable.

3.0 Energy considerations

3.1 Definition of the crack driving force

3.1.1 Linear-elastic material behaviour

In case of linear-elastic fracture mechanics the energy release rate G - called the crack driving force - is defined as the virtual change of potential energy δU_p available for a virtual crack-area increment $B\,\delta a$ and is directly related to the stress intensity factor by

$$G_I = \frac{\delta U_p}{B\,\delta a} = \frac{K_I^2}{E'} \tag{3.1}$$

In order to separate loading quantities which are related to *virtual* crack extensions from energy consumptions during real crack extensions we will use in this section as a special notation for the virtual crack changes the symbol δ.
The potential energy consists on the virtual work δA done by the external load and the virtual change of the elastically stored energy in the component δU:

$$\delta U_p = -\delta U + \delta A \quad , \quad \delta A = P\,\delta\delta_{LP} \tag{3.2}$$

In the sense of eq.(3.1) G is a loading quantity (not a material property) and up to now not related to real crack extensions da. In case of a real crack extension the energy dW_{crack} is necessary to create the new crack increment Bda. The energy per crack area increment defines the material property called "crack resistance" R

$$R = \frac{1}{B}\frac{dW_{crack}}{da} \tag{3.3}$$

The condition for maintaining crack propagation is expressed by

$$G = R \tag{3.4}$$

The left-hand side describes the available energy and the right-hand side the necessary energy.

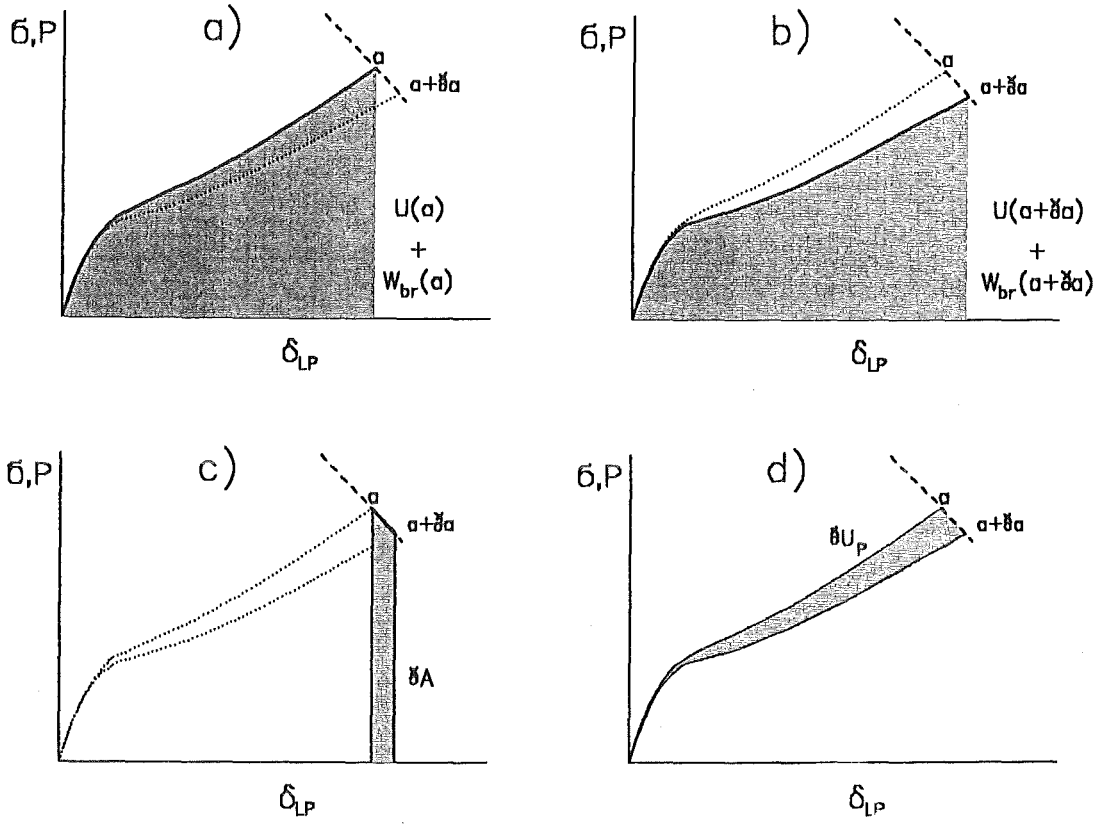

Figure 4. . Energy portions for specimens with crack lengths a and $a + \delta a$: a) elastically stored energy for a crack of length a; b) elastically stored energy for a crack of length $a + \delta a$; c) work increment done by the external load; d) increment of potential energy.

3.1.2 Nonlinear-elastic material behaviour

If nonlinear material behaviour plays a role - this is the case in the presence of strongly nonlinear bridging stresses - the relations of linear-elastic fracture mechanics have to be replaced by the J-integral concept. In order to apply J-integral we have to consider that the energy stored in the bridges W_{br} is **elastically stored energy** and therefore completely reversible. In this state it is not of importance what the real material response during unloading would be as long as no real displacement reversals occur. Here it should be emphasized once more that the J-integral is a loading quantity and not influenced by real material behaviour. Under these circumstances the virtual change of potential energy is

$$\delta U_p = \delta A - \delta W_{br} - \delta U \quad , \quad \delta A = P\,\delta\delta_{LP} \tag{3.5}$$

The virtual energy contributions are illustrated in fig.4. For nonlinear elastic material behaviour the loading quantity is

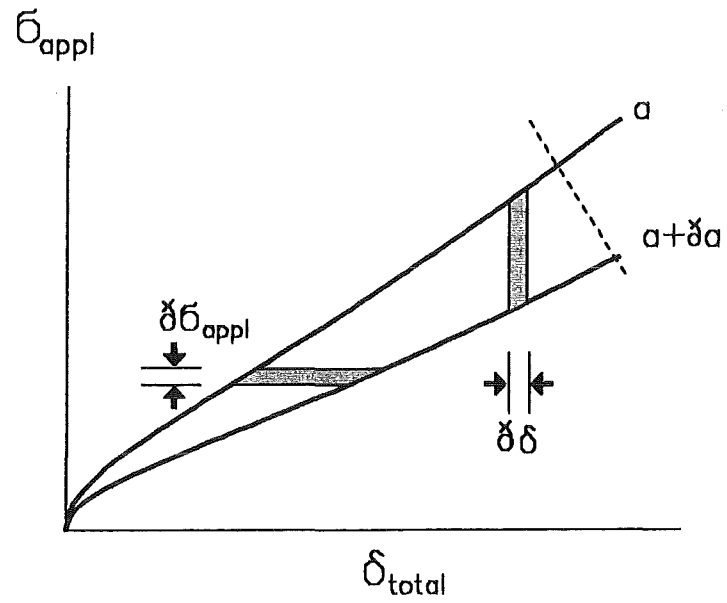

Figure 5. . Energy increments according to eqs.(3.9) and (3.10).

$$J = \frac{\delta U_p}{B\,\delta a} \tag{3.6}$$

and by definition $G = J = K_I^2/E'$ for the linear elastic case.
From eq.(3.1) and (3.5) it results for the J-integral [7]

$$J = -\int_0^{\delta_{LP}} \left(\frac{\delta P}{\delta a}\right)_{\delta'_{LP}} d\delta'_{LP} \tag{3.7}$$

$$J = \int_0^{P} \left(\frac{\delta \delta'_{LP}}{\delta a}\right)_{P'} dP' \tag{3.8}$$

and by using eq.(2.7)

$$J = -2\int_0^a dx \int_0^{\delta_{total}} \left(\frac{\delta \sigma'_{appl}}{\delta a}\right)_{\delta'_{total}} d\delta'_{total} \tag{3.9}$$

$$J = 2\int_0^a dx \int_0^{\sigma_{appl}} \left(\frac{\delta \delta'_{total}}{\delta a}\right)_{\sigma'_{appl}} d\sigma'_{appl} \tag{3.10}$$

Figure 5 shows the related potential energy dU_p.

3.1.3 Stress intensity factors, J-integral and energy release rate

If we introduce $\delta_{total} = \delta_{appl} + \delta_{br}$ in eq.(3.10)

$$J = 2\int_0^a dx \int_0^{\sigma_{appl}} \left[\left(\frac{\eth \delta'_{appl}}{\eth a} \right)_{\sigma'_{appl}} + \left(\frac{\eth \delta'_{br}}{\eth a} \right)_{\sigma'_{appl}} \right] d\sigma'_{appl} \tag{3.11}$$

and applying eq.(2.2) in the form

$$\frac{\eth \delta_{appl}}{\eth a} = \frac{K_{appl}\, h(x,a)}{E'} \tag{3.12}$$

we obtain

$$J = 2\int_0^a \frac{h(x,a)}{E'} dx \int_0^{\sigma_{appl}} K'_{appl}\, d\sigma'_{appl} + 2\int_0^a dx \int_0^{\sigma_{appl}} \left(\frac{\eth \delta'_{br}}{\eth a} \right)_{\sigma'_{appl}} d\sigma'_{appl} \tag{3.13}$$

Since

$$K'_{I\,appl} = \frac{K_{I\,appl}}{\sigma_{appl}}\, \sigma'_{appl} \tag{3.14}$$

the first term in (3.13) can be evaluated

$$J = \int_0^a \frac{h(x,a)}{E'}\, \sigma_{appl}\, K_{I\,appl}\, dx + 2\int_0^a dx \int_0^{\sigma_{appl}} \left(\frac{\eth \delta'_{br}}{\eth a} \right)_{\sigma'_{appl}} d\sigma'_{appl} \tag{3.15}$$

and after introduction of eq.(2.3) into the first term

$$J = \frac{1}{E'} K^2_{I\,appl} + 2\int_0^a dx \int_0^{\sigma_{appl}} \left(\frac{\eth \delta'_{br}}{\eth a} \right)_{\sigma'_{appl}} d\sigma'_{appl} \tag{3.16}$$

Since the second term in eq.(3.16) will vanish only in the case of cracks without bridging stresses we can conclude that the Irwin formula - written in terms of the applied stress intensity factor $K_{I\,appl}$ - is not generally valid

$$J \neq \frac{K_{I\,appl}^2}{E'} \tag{3.17}$$

This inequality holds for the general case without special assumptions made on the bridging stresses.

3.1.4 Special assumption on bridging stresses

Now a special assumption is made on the bridging stresses. It is physically meaningful to assume that the bridging stresses are only dependent on the actual crack opening diplacements (δ_{total})

$$\sigma_{br} = f(\delta_{total}) \tag{3.18}$$

and, for instance, not explicitly on the x-coordinate. Furthermore, it is assumed that this stress vs. displacement relation is a unique law for monotonically increasing displacements. The question whether or not the bridging-stress relation may change in unloading situations, i.e. in situations where the displacements can decrease, is without importance to the present considerations, since in controlled fracture tests the crack opening displacements increase monotonocally during crack extension.
This fact can easily be concluded from the weight function relation (2.2). In controlled fracture tests crack propagation occurs at $K_{total} = K_{I\,tip} = K_{I0}$. From (2.2) we conclude that for any given value of x - since $h(x,a) > 0$ - for all $0 \leq x < a$

$$\frac{\partial \delta_{total}}{\partial a}\Big|_{K_{total} = K_{I0}} = \frac{K_{I0}}{E'}\, h(x,a) > 0 \tag{3.19}$$

i.e. a monotonic increase in COD with increasing crack length.
Introducing eq.(2.5) into (3.9) gives

$$J = -2\int_0^a dx \int_0^{\delta_{total}} \left[\left(\frac{\partial \sigma'_{total}}{\partial a} \right)_{\delta'_{total}} - \left(\frac{\partial \sigma'_{br}}{\partial a} \right)_{\delta'_{total}} \right] d\delta'_{total} \tag{3.20}$$

If σ'_{br} is a unique function of δ'_{total}, one can write for the second term in brackets (since δ'_{total} is kept constant)

$$\left(\frac{\partial \sigma'_{br}}{\partial a} \right)_{\delta'_{total}} = 0 \tag{3.21}$$

and (3.20) reduces to

$$J = -2\int_0^a dx \int_0^{\delta_{total}} \left(\frac{\partial \sigma'_{total}}{\partial a} \right)_{\delta'_{total}} d\delta'_{total} \tag{3.22}$$

After integration by parts (see fig.5 and replace the vertical axis by σ_{total}) this reads

$$J = 2\int_0^a dx \int_0^{\sigma_{total}} \left(\frac{\delta \delta'_{total}}{\delta a} \right)_{\sigma'_{total}} d\sigma'_{total} \tag{3.23}$$

and with eq.(2.2), written in the form

$$\frac{\delta \delta_{total}}{\delta a} = \frac{K_{total}\, h(x,a)}{E'} \tag{3.24}$$

we obtain

$$J = 2\int_0^a dx \int_0^{\sigma_{total}} \frac{K'_{total}}{E'} h(x,a)\, d\sigma'_{total} \tag{3.25}$$

Changing the order of integration results in

$$J = \frac{2}{E'} \int_0^{K_{total}} K'_{total}\, dK'_{total} = \frac{K^2_{total}}{E'} = G \tag{3.26}$$

Since during crack propagation the crack-tip stress intensity factor equals K_{I0}, we finally can write

$$G_{I0} = J_0 = \frac{K_{I0}^2}{E'} \tag{3.27}$$

The authors confess that this relation seems nearly self-evident. But it should be taken into account that in contrast to the original derivation here nonlinear loaded surfaces are considered.

3.2 The crack resistance

3.2.1 Energy balance during crack propagation

During stable crack propagation the externally applied force P performs the mechanical work A, which is identical with the area under the load-displacement curve

$$A = \int_0^{\delta_{LP}} P'\, d\delta'_{LP} \tag{3.29}$$

This energy equals the sum of

- the elastically stored energy in the specimen U,
- the energy necessary to create a new fracture surface W_{crack}, and

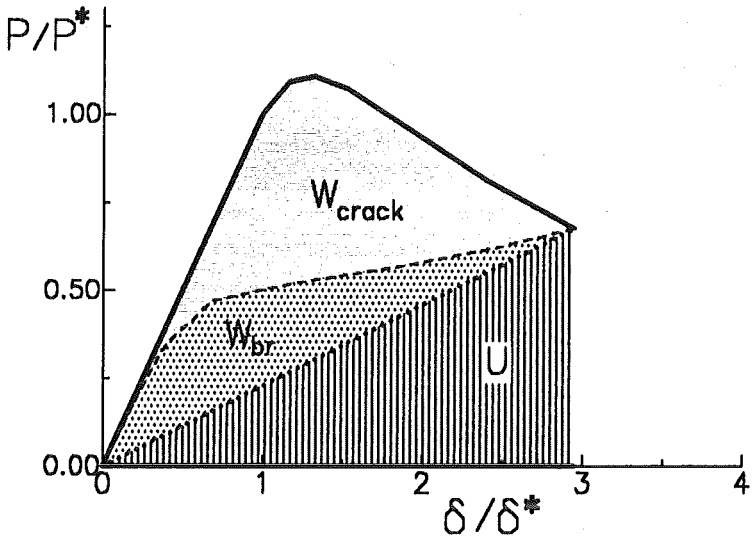

Figure 6. . Global energies for a cracked component under tesion; Load and loading-point displacement normalised on the values at the onset of stable crack extension (*); calculated with eqs.(A1) and (A2) for $a_0/W = 0.5$

- the energy deposit in the bridges W_{br},

i.e.

$$A = U + W_{crack} + W_{br} \tag{3.30}$$

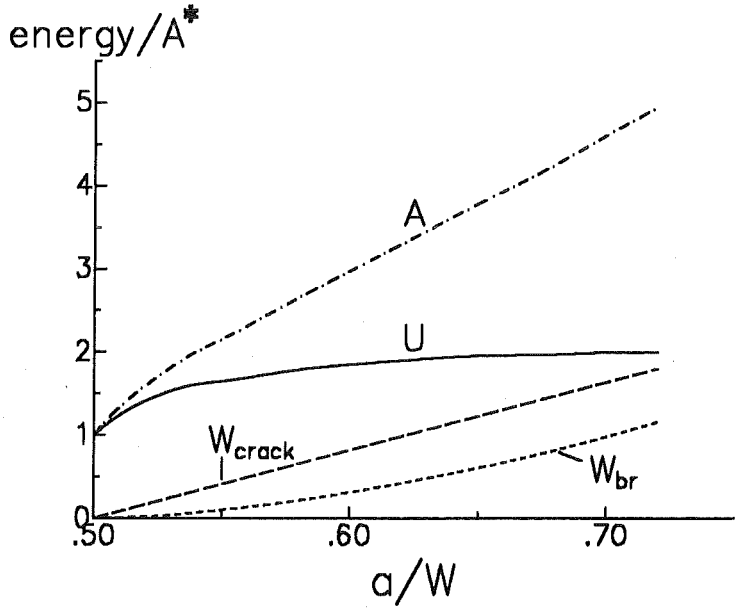

Figure 7. . Energy contributions during stable crack propagation; $A^* = P^*\delta^*/2$, loading case: tension.

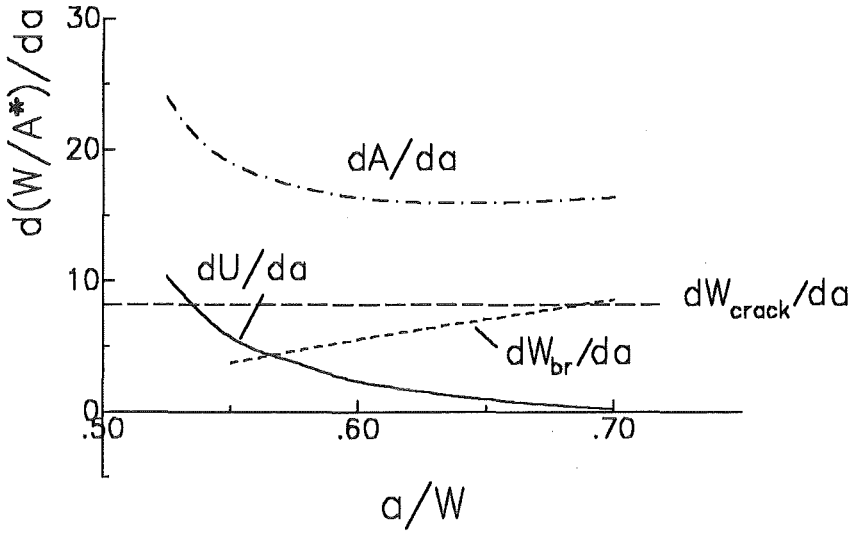

Figure 8. . Energy rates according to fig.7.

The energy necessary to create a new crack surface is

$$W_{crack} = \frac{K_{I0}^2}{E'}(a - a_0) \tag{3.31}$$

and the energy consumed in the bridges is given by

$$W_{br} = -2B \int_0^a dx \int_0^{\delta_{total,c}} \sigma'_{br}\, d\delta'_{total} \quad ; \quad \sigma_{br} < 0 \tag{3.32}$$

In the special case of the exponential relation (A1+A2) the inner integral can be evaluated and it results

$$W_{br} = -2B\,\sigma_0\delta_0 \int_0^a [1 - \exp(-\delta_{total,c}/\delta_0)]\, dx \quad ; \quad \sigma_0 < 0 \tag{3.33}$$

The elastically stored energy U in the specimen is given by (see fig.6)

$$U = \frac{1}{2} P\, \delta_{LP} \tag{3.34}$$

in a simple way from the applied load and the loading point displacement. The different energy contributions are plotted in fig.7 versus the crack extension $\Delta a = a - a_0$ for tension as the loading case. For the first numerical calculations represented in figs.6-8 a bridging relation $\sigma_{br} = \sigma_0 \exp(-\delta/\delta_0)$ with $\sigma_0 = K_{I0}/\sqrt{W}$ and $\delta_0 = 5/6 \cdot (\sigma_0 W/E')$ was used. Whilst the "bridging energy" W_{br} and the crack surface energy W_{crack} increase monotonically with crack extension, the elastic energy seems to reach a saturation. The incremental energies dA/da, dW_{br}/da, dW_{crack}/da, and dU/da are plotted in fig.8. dU/da may change its sign at $a/W > 0.7$.

In the linear-elastic case with unloaded crack faces the crack resistance was defined by the energy that has to be provided to create new crack surface. In the presence of bridging stresses an additional energy has to be provided to overcome the attracting bridging stresses. The energy balance now reads

$$\frac{dA}{da} - \frac{dU}{da} - \frac{dW_{br}}{da} = \frac{dW}{da} \tag{3.35}$$

or

$$G = \frac{dU_p}{B\,da} = \frac{dW}{B\,da} = R^* \tag{3.36}$$

The changing energy in the bridges then is part of the **available** energy for crack extension. Alternatively it can be written

$$\frac{dA}{B\,da} - \frac{dU}{B\,da} = \frac{dW_{br}}{B\,da} + \frac{dW}{B\,da} = R \tag{3.37}$$

Then the changing energy in the bridges is part of the energy consumption and therefore included in R. Consequently, the crack growth resistance now reads

$$R = \frac{1}{B}\left(\frac{dW_{crack}}{da} + \frac{dW_{br}}{da}\right) = \frac{K_{I0}^2}{E'} + \frac{1}{B}\frac{dW_{br}}{da} \tag{3.38}$$

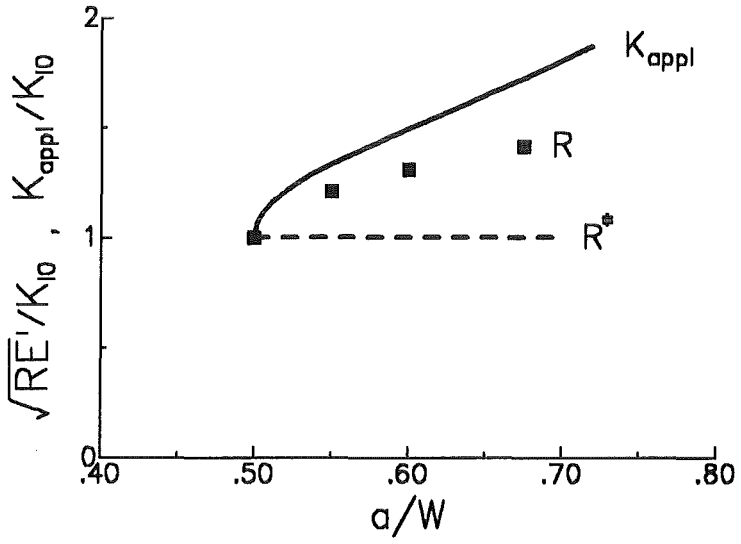

Figure 9. . Applied stress intensity factor $K_{I\,appl}$ and crack resistance R (expressed in terms of stress intensity factor) for the tensile loading case, computed with the bridging stress relation $\sigma_{br} = \sigma_0 \exp(-\delta/\delta_0)$; R^*: eq.(3.36), R: eq.(3.38).

3.2.2 The crack resistance and the applied stress intensity factor

It can easily be shown that the applied stress intensity factor $K_{I\,appl}$ and the crack resistance R cannot be converted by eq.(1.2) in the general case. For the further conclusions we consider the tensile loading case. We express the term $K_{I\,appl}^2/E'$ by definition of the weight function in the form

$$h(x,a) = \frac{E'}{K_{I\,appl}} \frac{\partial}{\partial a} \delta_{appl}(x,a) \tag{3.39}$$

as

$$\frac{1}{E'} K_{I\,appl}^2 = \frac{K_{I\,appl}}{E'} \int_0^a h(x,a)\sigma_{appl}\, dx = \int_0^a \sigma_{appl} \frac{\partial \delta_{appl}}{\partial a}\, dx \tag{3.40}$$

Introducing eq.(2.7) yields

$$\frac{1}{E'} K_{I\,appl}^2 = \frac{1}{2B} P \frac{\partial \delta_{LP,appl}}{\partial a} \tag{3.41}$$

The loading point displacements $\delta_{LP,appl}$ can be written

$$\delta_{LP,appl} = \delta_{LP,total} - \delta_{LP,br} = \delta_{LP,total} + |\delta_{LP,br}| \tag{3.42}$$

and consequently

$$\begin{gathered} \frac{1}{E'} K_{I\,appl}^2 \neq \frac{1}{2B} P \frac{\partial \delta_{LP,total}}{\partial a} \\ \frac{1}{E'} K_{I\,appl}^2 \neq R \end{gathered} \tag{3.43}$$

In cases where the bridging zone increases with increasing crack length (before a saturation in R is reched) we will find

$$d(\delta_{LP,appl}) > d(\delta_{LP,total}) \quad \rightarrow \quad \frac{1}{E'} K_{I\,appl}^2 > R \tag{3.44}$$

As an example the applied stress intensity factor $K_{I\,appl}$ and the crack resistance R have been computed numerically for a component under tensile loading containing a crack of initial length $a/W = 0.5$. The results of R are formally expressed in terms of stress intensity factors and plotted in fig.9. The disagreement of the two quantities is clearly obvious.

3.3 Application of a Dugdale model by Evans and McMeeking

In a simple model Evans and McMeeking [9] considered the conversion of energy release rates in stress intensity factors in a special model. They studied a small scale bridging zone in a brittle material reinforced by fibers (see fig.10). In the following the nomenclature of [9] will be used. The crack surface stresses transferred by the fibres are considered to be homogeneously distributed in the bridged crack area. The maximum size of the bridging zone is D_c where the subscript refers to the critical situation at the crack tip, i.e. $K_{I\,tip} = K_{I0}$.
From the J-integral around the traction zone the critical value of the change in energy release rate $\Delta\mathbf{G}$ is derived as

$$\Delta\mathbf{G}_c = 2\sigma f u_c \tag{3.46}$$

with the tractions in the fibers σ, the area fraction f of reinforcements on the crack plane and u_c the critical crack opening at the end of the bridging zone, given by

$$u_c = \frac{4(1-\nu)}{G}\left(\frac{f\sigma D_c}{\pi} + \frac{K_{I0}\sqrt{D_c}}{G\sqrt{2\pi}}\right) \tag{3.47}$$

where G is the shear modulus and K_{I0} is the critical crack-tip stress intensity factor.
The contribution of the bridging zone to the stress intensity factor results with the near-tip weight function as

$$\Delta K_I = -\sqrt{\frac{2}{\pi}}\, f \int_0^{D_c} \frac{\sigma(x)}{\sqrt{x}}\, dx \tag{3.48}$$

where x is the distance from the crack tip. The "change in fracture toughness" ΔK_c results from eq.(3.48) as

$$\Delta K_c = 2\sigma f \sqrt{2D_c/\pi} \tag{3.49}$$

The following *definitions* are introduced

$$\frac{2G\mathbf{G}_c}{1-\nu} = K_c^{\,2} \tag{3.50}$$

$$K_c = K_{I0} + \Delta K_c \tag{3.51}$$

$$\mathbf{G}_c = \mathbf{G}_0 + \Delta\mathbf{G}_c \tag{3.52}$$

In the opinion of the authors eqs.(3.51) and (3.52) are definitions of the quantities K_c and $\mathbf{G}_c$. On the other hand there is no additional freedom to *define* a relation between the two quantities of type eq.(3.50). The validity of eq.(3.50) has to be proved.
If we assume eq.(3.50) would be correct, it results by combining eqs.(3.50) to (3.52) yielding

$$2G\Delta\mathbf{G}_c/(1-\nu) = (\Delta K_c)^2 + 2K_{I0}\Delta K_c \tag{3.53}$$

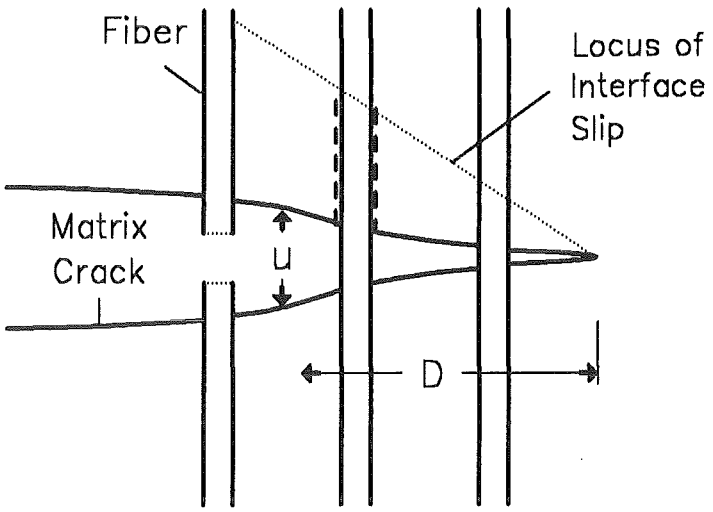

Figure 10. Bridging zone in reinforced materials. Bridging zone for slipping fibers according to Evans and McMeeking [9].

Introducing of eq.(3.46) and eq.(3.47) at the left side of (3.53) and eq.(3.49) at the right hand side it results that the left-hand side is twice the right-hand side.
The reason is a typing error in eq.(3.46) since

$$J = \sigma \cdot COD \quad \rightarrow \quad \Delta \mathbf{G}_c = \sigma f u_c \tag{3.54}$$

The analysis of Evans and McMeeking confirms the correctness of relation (3.50) for a special case, namely the **small-scale bridging** and the **steady-state behaviour** of a growing crack in an infinite body with a small bridging zone of constant length behind the crack tip. But this consideration is not a general prove of eq.(3.53).
In this special case it holds (in notation of the previous sections)

$$\int_{(crack)} \delta_{br}(x)\, dx = const.$$

$$\rightarrow \quad \frac{d}{da} \int_{(crack)} \delta_{appl}(x)\, dx = \frac{d}{da} \int_{(crack)} \delta_{total}(x)\, dx \tag{3.55}$$

and from the considerations made before we can conclude

$$\left(\frac{1}{E'} K_{I\,appl}^2 \right)_{steady-state} = R_{steady-state} \tag{3.56}$$

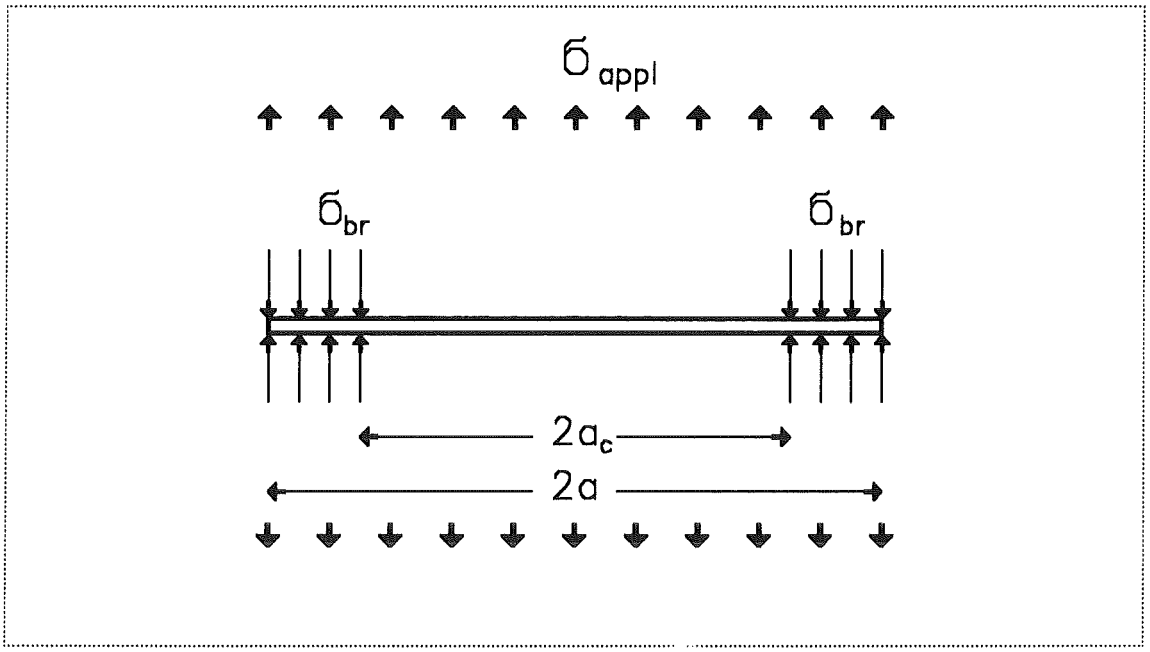

Figure 11. . Griffith crack with constant bridging stresses; loading situation and geometry.

3.4 R-curve for a Griffith crack with constant bridging stresses

A restriction of the model used by Evans and McMeeking is that an approximate weight function has to be used which becomes correct only in the limit case of an infinitely large crack compared with the dimension of the bridging zone. In order to investigate the relation between crack resistance and applied stress intensity factor it is useful to apply an analytically exact solution.

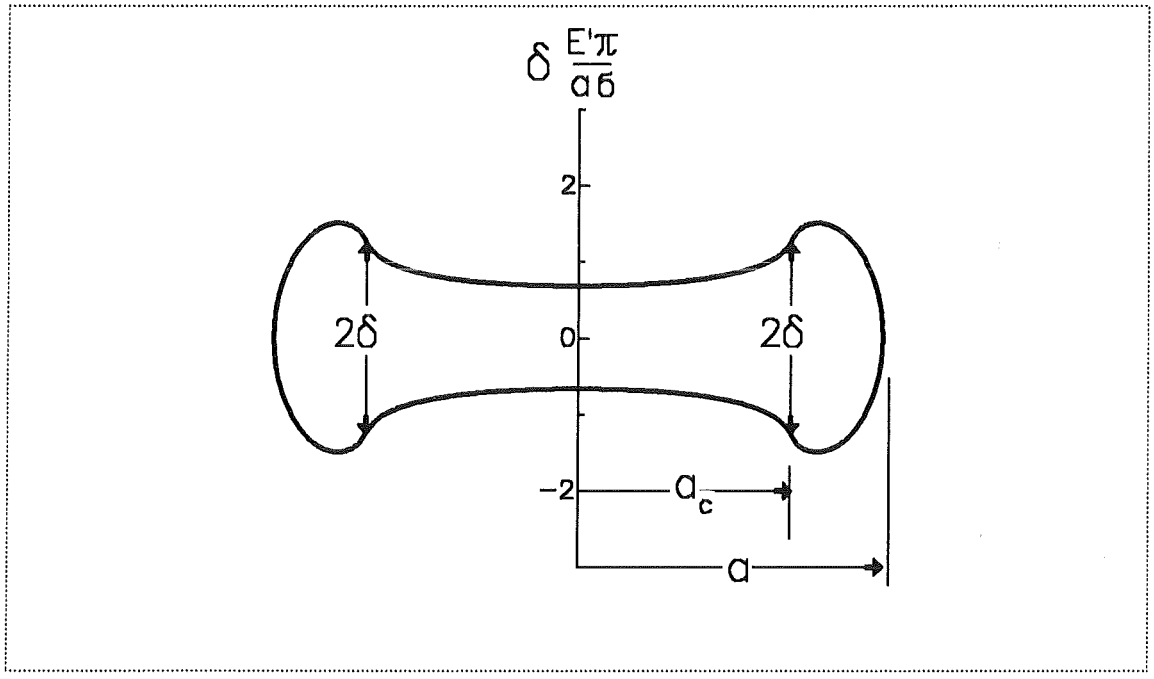

Figure 12. . Griffith crack with constant bridging stresses; displacemet field caused by the strip load.

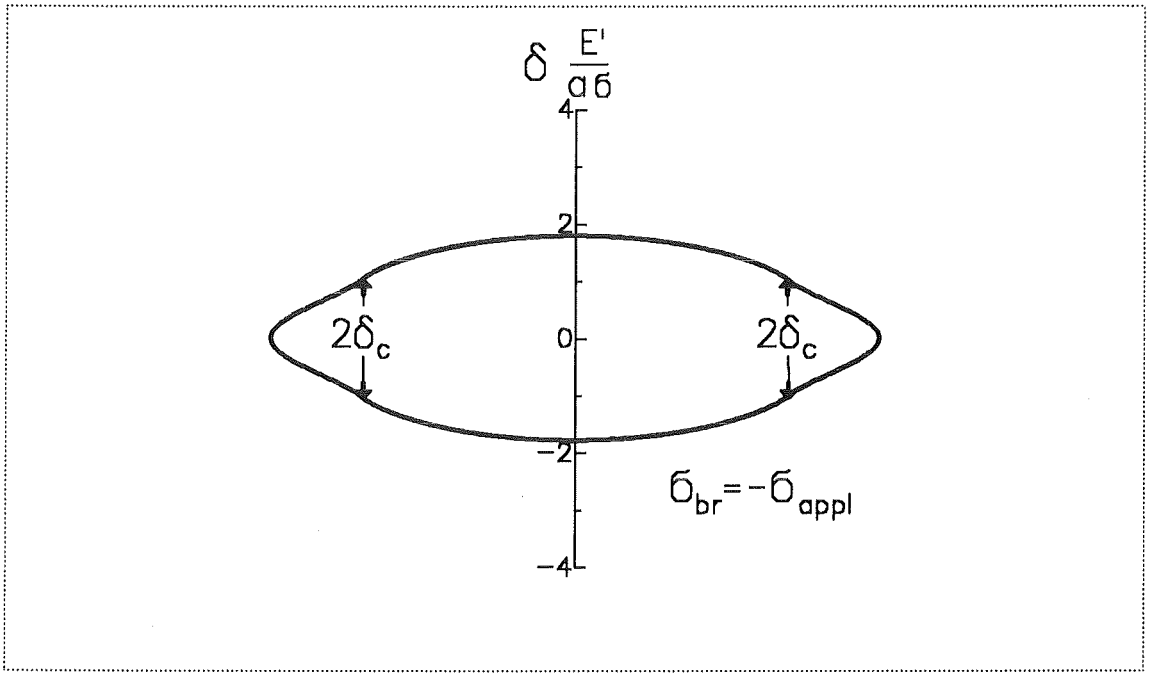

Figure 13. . Griffith crack with constant bridging stresses; total displacemet field.

Let us consider a Griffith crack (a straight through-the-thickness crack) of size $2a$ in an infinite body which is symmetrically loaded in the range $a_c < |x| < a$ by a constant stress σ. Figure 11 illustrates geometry and loading conditions. The displacements under this strip load are given by eq.(2.4) and the weight function reads

$$h(x,a) = \frac{2}{\sqrt{\pi a}} \frac{a}{\sqrt{a^2 - x^2}} \tag{3.57}$$

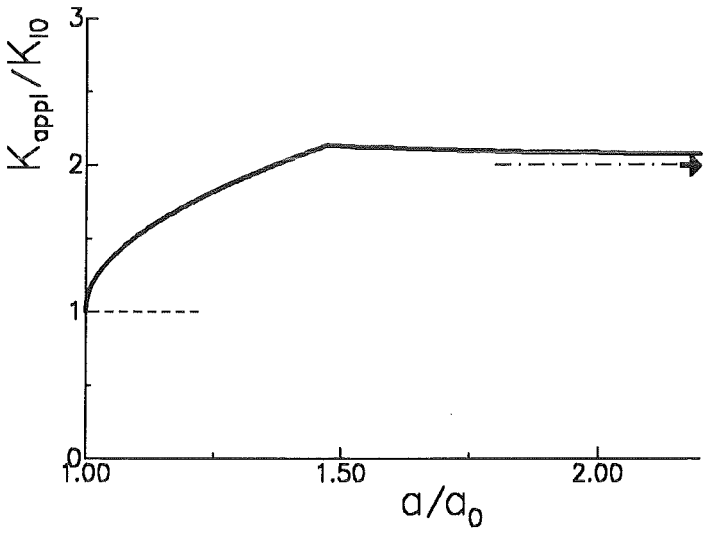

Figure 14. . R-curve for a Griffith crack with bridging stresses σ = constant.

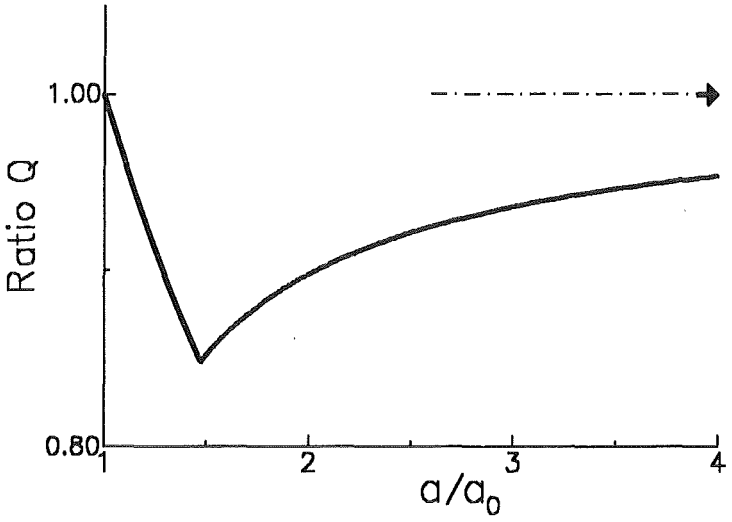

Figure 15. . Ratio of crack resistance and stress intensity factors according to eq.(3.67).

We find for the crack opening displacement field according to [10]

$$\delta(x,a) = \frac{\sigma a}{E'\pi}\left[4\theta \sin\varphi - \cos\varphi \cdot \ln\frac{\sin^2(\theta-\varphi)}{\sin^2(\theta+\varphi)} - 2\cos\theta \cdot \ln\frac{\sin\theta+\sin\varphi}{\sin\theta-\sin\varphi}\right] \tag{3.58}$$

$$\theta = \arccos(a_0/a) \quad , \quad \varphi = \arccos(x/a) \tag{3.59}$$

as plotted in fig.12. The related bridging stress intensity factor results as

$$K_{Ibr} = \sigma 2\sqrt{a/\pi}\int_{a_c}^{a}\frac{dx}{\sqrt{a^2-x^2}} = 2\sigma\sqrt{\frac{a}{\pi}}\left[\frac{\pi}{2} - \arcsin(a_c/a)\right] \tag{3.60}$$

The crack opening displacement field caused by the applied stresses σ_{appl} is

$$\delta(x,a) = 2\frac{\sigma_{appl}}{E'}\sqrt{a^2-x^2} \tag{3.61}$$

and the applied stress intensity factor $K_{I\,appl}$ is given as

$$K_{I\,appl} = \sigma_{appl}\sqrt{\pi a} \tag{3.62}$$

The total crack opening displacement field follows from the superposition of eqs.(3.58) and (3.61), and the total stress intensity factor from superposition of eqs.(3.60) and (3.62). Figure 13 shows the total crack opening displacement field for $|\sigma|/\sigma_{appl}=1$.
For the calculation of the R-curve it is assumed that a critical crack opening displacement δ_c exists at which the bridging interactions become abruptly dissolved, i.e. $\sigma_{br}=0$ for $\delta > \delta_0$. Now we can determine the R-curve numerically from the two conditions:

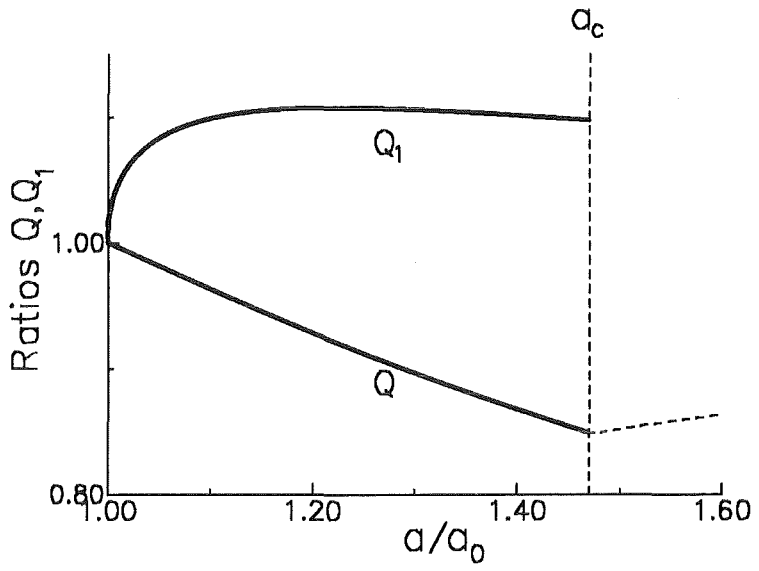

Figure 16. . Ratio of crack resistance and stress intensity factors according to eqs.(3.67) and (3.69) for the first phase of crack extension $a \leq a_c$.

1. The total stress intensity factor must coincide with K_{I0}

$$\sigma_{appl}\sqrt{\pi a} - |\sigma_{br}|2\sqrt{\frac{a}{\pi}}\left[\frac{\pi}{2} - arcsin(a_c/a)\right] = K_{I0} \tag{3.63}$$

2. At the end of the bridging zone the critical crack opening displacement must be reached

$$2\frac{\sigma_{appl}}{E'}\sqrt{a^2 - x^2} - |\delta_{br}| = \delta_c \tag{3.64}$$

The solution of these two relations results in σ_{appl} and a_c for a given crack length a. From σ_{appl} the stress intensity factor $K_{I\,appl}$ can be calculated. An R-curve resulting for a crack of initial crack length a_0 is represented in fig.14. The calculation of the R-curve was performed in the following way. A crack of initially unbridged length $a = a_0$ is considered. The applied stress is increased up to a certain value that satisfies the condition for the onset of stable crack extension, namely

$$K_I = \sigma_{appl}\sqrt{\pi a_0} \tag{3.65}$$

Then a is increased as long as $\delta(x = a_0) < \delta_c$. The applied stress intensity factor results from eq.(3.63) as

$$K_{I\,appl} = K_{I0} + |\sigma_{br}|2\sqrt{\frac{a}{\pi}}\left[\frac{\pi}{2} - arcsin(a_0/a)\right] \tag{3.66}$$

During further crack extension it results $a_c > a_0$ and the solution of eqs.(3.63) and (3.64) can be found with a zero routine. The R-curve, resulting for $\delta_c E'/(|\sigma_{br}|a_0) = 1.5$ is plotted in fig.14. The R curve starts very steep like $K_{br} \propto \sqrt{a - a_0}$ and after δ_c is reached (in the plotted example at $a = 1.47a_c$) the applied stress intensity factor decreases slightly against the asymptotic value of $K_{I\,appl}/K_{I0} = 2$. The crack resistance obtained with eq.(3.46) has been plotted in fig.15 in a normalised representation according to eq.(3.53) as the ratio

$$Q = \frac{E'J}{K_{Ibr}^2 + 2|K_{Ibr}|\, K_{I0}} \tag{3.67}$$

This ratio should be $Q = 1$ if the Irwin equation would be valid in the presence of an R-curve behaviour. From fig.15 we find that at the onset of crack extension the ratio is $Q = 1$. In this situation the bridging zone is negligible in size compared with the initial crack length a_0. Then we detect a significant deviation from the value $Q = 1$ and after very long crack propagation, when the bridging zone of finite length is again small compared with the crack length, the ratio Q tends asymptotically against $Q = 1$.
If we consider the work done by the external load against the constant bridging stresses we can write for $a < a_c$

$$W_{br} = \sigma \int_{a_0}^{a} 2\delta(x)\, dx \tag{3.68}$$

that allows to define the ratio

$$Q_1 = \frac{dW_{br}/da}{K_{Ibr}^2 + 2|K_{Ibr}|\, K_{I0}} \tag{3.69}$$

Figure fig.16 illustrates the two ratios Q, Q_1 for $a \leq a_c$. The second ratio Q_1 also deviates from the value $Q = 1$ but will asymptotically tend against this limit value.

3.5 Conclusions

From the previous considerations one can conclude:

1. If the energy release rate is defined by eqs.(3.1) and (3.2) and the crack resistance by eq.(3.3) it results that $G_{I0} = K_{I0}^2/E'$ where G_{I0} is that characteristical value of G that governs onset of stable crack growth.

2. If the energy release rate and the crack resistance are defined by eqs.(3.35)-(3.38) one can show that the Irwin relation in general does not hold for the applied stress intensity factor, i.e. $K_{I\,appl}^2/E' \neq R$.

3. On the other hand the analysis of Evans and McMeeking [9] ensures the validity of eq.(1.2) for the special case of small-scale bridging. From a simple example the deviations become obvious if crack and bridging zone are comparable in size.

4.0 Compliance and R-curve

4.1 Compliance

4.1.1 Loading-point compliance

The compliance of a cracked specimen is defined as the relative displacement of the loading points δ_{LP} divided by the load applied

$$C = \frac{\delta_{LP}}{P} \tag{4.1}$$

The compliance is applied in fracture mechanics

- for the determination of the actual crack depth, and
- for the computation of energy release rates from load vs. displacement curves resulting in controlled fracture tests.

In case of a crack in a component with crack faces completely free of stresses the compliance is directly related to the crack depth. Under pure tensile loading it holds

$$C = C_0 + \frac{2}{BE'} \int_0^{\alpha} Y^2(\alpha')\, \alpha'\, d\alpha' \quad , \quad \alpha = a/W \tag{4.2}$$

where Y is the geometric function for the stress intensity factor calculation, defined by

$$K = \sigma_{appl}\, Y \sqrt{a} \tag{4.3}$$

which can be taken from handbooks.
In the presence of bridging stresses at the crack faces deviations in the compliance have to be expected [11]. Due to the bridging stresses, the specimens' stiffness is greater than that obtained for specimens with completely free crack surfaces, i.e. the crack length resulting from compliance measurements will be lower than the real physical crack length.
Equations (2.6) and (2.7) provide the possibility of computing a differential compliance C_{diff} which gives the increment of displacement for a given increment of load (or stress applied)

$$C_{diff} = \frac{d\delta_{LP}}{dP} \tag{4.4}$$

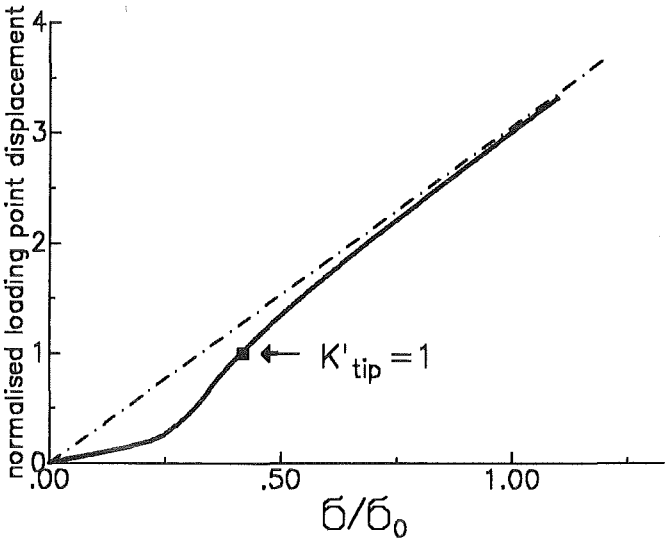

Figure 17. . Loading point displacements as a function of load, calculated with eq.(A1 + A5) for $a/W = 0.7$; dash-dotted straight line: displacements for the elastic case with interaction-free crack surfaces, dotted straight line: limit case for $a/W = 0.5$.

whilst the global compliance C_{glob} is defined by eq.(4.1).
For numerical calculations the bridging stress relations given in the Appendix are used in the following. In order to allow dimensionless computations to be made, the numerical results for the stress intensity factors and displacements are normalised by the characteristic bridging stress σ_0 and the specimen width W according to

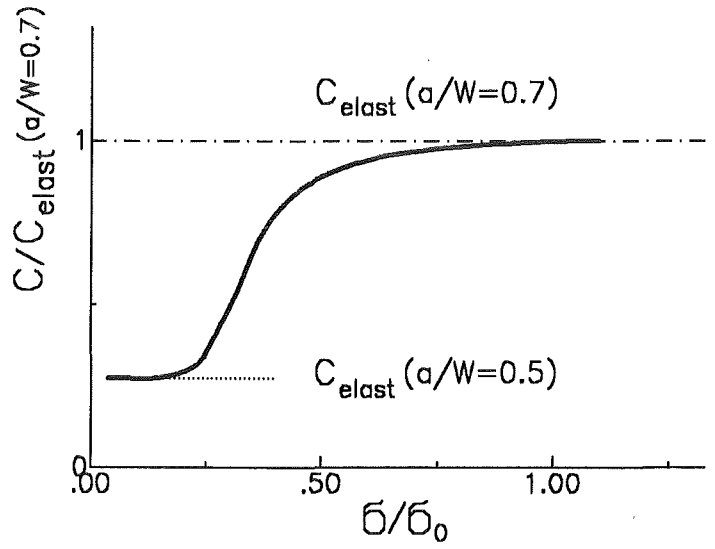

Figure 18. . Global loading-point compliance, calculated with eq.(A1 + A5) for $a/W = 0.7$; dash-dotted straight line: limit case for interaction-free crack with $a/W = 0.7$; dotted straight line: compliance of an interaction-free crack with $a/W = 0.5$.

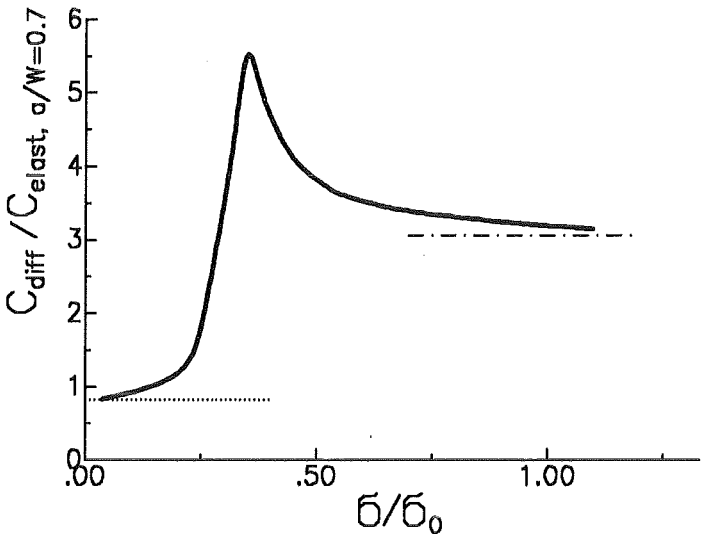

Figure 19. . Differential compliance according to (4.4) derived from the data of fig.17.

$$K' = \frac{K}{\sigma_0\sqrt{W}} \quad , \quad \delta' = \frac{\delta E'}{\sigma_0 W} \tag{4.5}$$

In fig.17 the loading-point displacements are plotted as a function of the stress applied. The displacements are normalised on that value that is reached at $K'_{tip}=1$. As can be seen from fig.17, most of the deviations between the loading-point displacements in the presence of bridging stresses and the displacements calculated ignoring these additional stresses (dash-dotted straight line) occur at lower loads. The higher the load, the smaller is the remaining bridging zone, and the influence of bridging stresses decreases. A lower limit of the displacements can

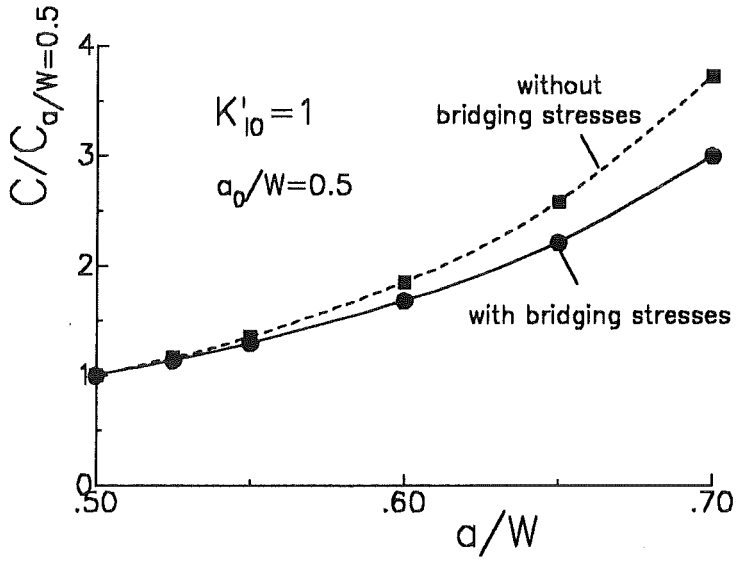

Figure 20. . Global compliance as a function of crack length for $K'_{I0}=1$.

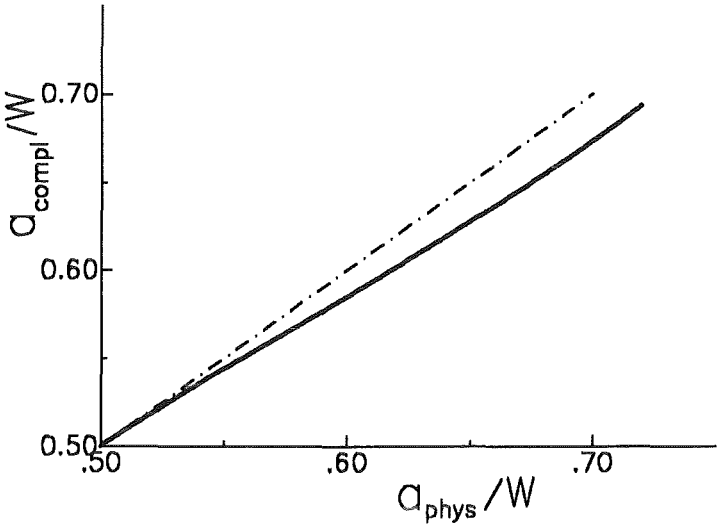

Figure 21. . Deviations between the physical crack depth a_{phys} and the apparent crack depth a_{compl} resulting from the compliance.

be calculated by considering only the initial crack size $a = a_0$. This limit case is introduced in fig.17 as a dotted straight line.
In fig.18 the total compliance is shown for a crack of $a/W = 0.7$ and $a_0/W = 0.5$. As expected from the non-linear bridging stress, the comliance is not constant. Under low loads the compliance in the presence of bridging stresses tends towards the compliance of a crack of length a_0/W without bridging stresses. At high loads the compliance tends asymptotically to the compliance of a crack of depth a/W without bridging stresses.
The differential compliance resulting from the results given in fig.18 is shown in fig.19. Significant deviations between differential compliance and global compliance are evident.
The total compliance of the whole crack-containing component is then given by

$$C_{total} = C_{glob} + C_0 \quad , \quad C_0 = \frac{2L}{EWB} \quad \text{for tension} \tag{4.6}$$

where C_0 is the compliance of the uncracked component. In fig.20 the compliance of the specimen in the presence of bridging stresses is represented together with the compliance in the absence of bridging interactions versus the actual crack size. It is obvious that the specimens with bridging interactions react more rigidly than the ideal fracture-mechanics specimens with completely free crack faces. Two types of crack depth can be concluded from fig.21, namely the real physical crack depth a_{phys} and the apparent crack depth a_{compl} which can be concluded from the compliance by application of pure linear-elastic relations. In the representation fig.20 one can also see that the real crack size is larger than that obtained from the compliance.

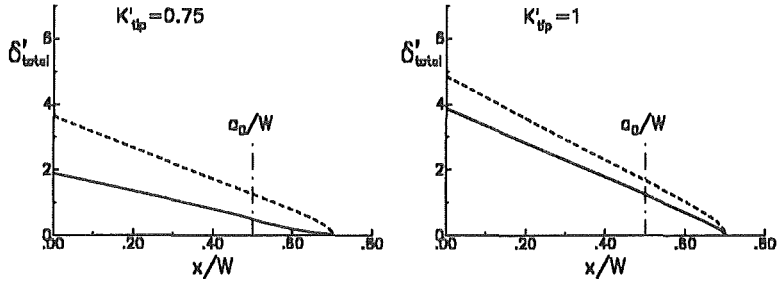

Figure 22. . Crack profile for a crack (in a bent plate) with bridging stresses in the range $a_0/W < x/W < a/W$; dashed curves: crack profiles in the absence of bridging stresses (loaded by the same applied stress intensity factor K'_{appl}).

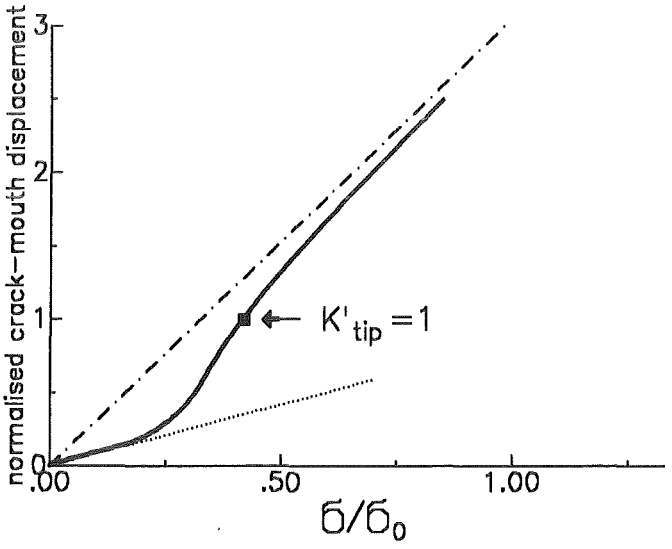

Figure 23. . Crack-mouth displacements as a function of load calculated with eq.(A1+A5) for $a/W = 0.7$; straight line: displacements for the elastic case with interaction free crack surfaces.

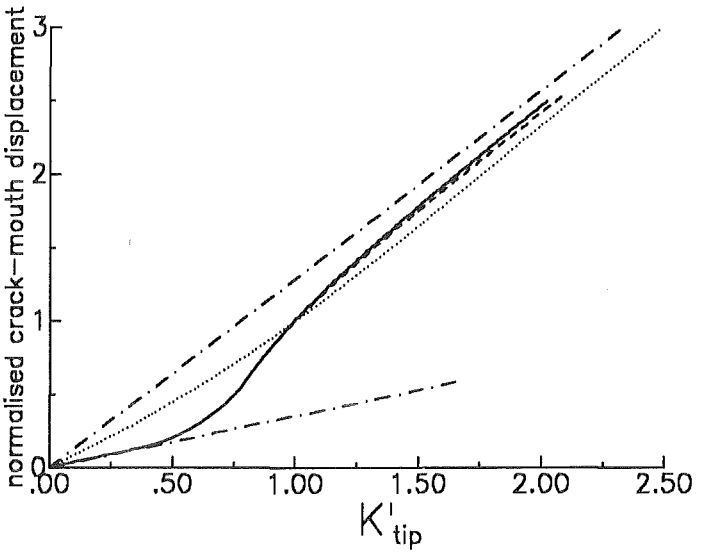

Figure 24. . Crack-mouth openings for a crack with $a_0/W=0.5$, $a/W=0.7$, calculated with different bridging stress relations; solid line: (A1 + A5), dashed line: (A1 + A2), dotted line (A11).

4.1.2 Crack-mouth compliance

A very popular possibility of indirect determination of the crack depth is the measurement of crack-mouth opening. The related crack-mouth compliance C_{CM} can be derived from the displacements δ_{CM} at the location $x = 0$ and the actual load P as

$$C_{CM} = \frac{\delta_{CM}}{P} \tag{4.7}$$

where the crack-mouth displacements may be determined from eq.(6) as

$$\delta_{CM} = \frac{1}{E'} \int_0^a \int_{x'}^a h(a',0)h(a', x') \left[\sigma_{appl}(x') + \sigma_{br}(x')\right] da'dx' \tag{4.8}$$

Figure 22 shows the crack profiles under different loads for cracks with and without bridging interactions in the region $a_0 < x < a$ for a crack with $a_0/W=0.5$, $a/W=0.7$. In fig.23 the crack-mouth displacements resulting from (4.8) are plotted for $a_0/W=0.5$, $a/W=0.7$ and the bridging stress relations given by eqs.(A1+A2), (A1+A5) and (A11) in the Appendix. A curve is obtained which is qualitatively identical to that for the loading-point displacements. Figure 24 represents the crack-mouth displacements for the three bridging relations used. In all cases the crack-mouth displacement underestimates the actual crack length, i.e. the curves run below the upper straight line.

4.2 R-curves

4.2.1 Calculation of R-curves

From the solution of eq.(2.6) the bridging stresses along the crack can be computed for a given applied stress σ_{appl}, and eqs.(2.3a) and (2.3b) provide the related stress intensity factors $K_{I\,appl}$ and K_{Ibr}. Since in a controlled frature test the crack-tip stress intensity factor $K_{I\,tip} = K_{total}$ is constant, namely $K_{I\,tip} = K_{I0}$, the R-curve $K_{I\,appl} = f(a - a_0)$ results from eq.(2.9) as

$$K_{I\,appl} = K_{I0} + |K_{Ibr}| \tag{4.9}$$

This correctly derived applied stress intensity factor $K_{I\,appl}$ will be denoted below as the real one. In fig.25 the entire R-curve is plotted for the bridging relation (A1+A5) given in the Appendix. Since K_{I0} is constant, K_{Ibr} reflects all further information on the R-curve behaviour.
In order to allow a comparison to be made with the influence of the shape of the bridging-stress relation, we will choose the parameters σ_0 and δ_0 in such a way that the maximum bridging stresses as well as the separation energies are identical in all cases. Figure 26 shows the bridging stress intensity factor K_{Ibr} as a function of the crack extension Δa in a normalised representation for the bridging relation (A1+A2) as solid curve, for relation (A1+A5) as dashed curve, and for eq.(A11) as dotted line.
It is obvious that the dependency of (A1+A2) is square-root shaped at the beginning of crack extension. Also (A1+A5) shows a strong increase at $\Delta a = 0$. The initial slope for spring-like bridging stresses (A11) is much less steep.

4.2.2 Experimental R-curves

A number of procedures are possible which yield different $K_{I\,appl}$ values. Several applied stress intensity factors will be defined below:

- Measurements of the true actual crack length a - for instance by use of a travelling microscope - and knowledge of the actual load P or stress $\sigma_{appl} = P/(BW)$ yield the stress intensity factor which is correct in terms of fracture mechanics

$$K_{I\,appl} = \sigma_{appl}\, Y(a)\, \sqrt{a} \tag{4.10}$$

- Very often, the actual crack length is concluded from the global compliance of the specimen, eq.(4.1), which increases with increasing crack length. This apparent crack length, denoted by a^*, is smaller than the real one ($a^* < a$). The related stress intensity factor, calculated with a^*,

$$\tilde{K}_{Iappl} = \sigma_{appl}\, Y(a^*)\, \sqrt{a^*} \tag{4.11}$$

  is consequently lower than the stress intensity factor calculated with a:

Combined with the Irwin formula, eq.(1.1), the energy release rate allows to define further stress intensity factors. The basis of such evaluations are the load-displacement curves. They can be measured as well as computed with eqs.(2.6) and (2.7). Computed curves are shown as examples in fig.27 for different crack lengths. The $P - \delta_{LP}$ –curves (or $\sigma_{appl} - \delta_{LP}$ –curves) which would result in a controlled fracture test are found from the curves in fig.27 as the stress-displacement combinations for which the condition $K_{I\,tip} = K_{I0}$ is fulfilled. From fig.27 the values for which K'_{tip} is equal to K'_{I0} were determined. For the following calculations $K'_{I0} = 1$ was chosen. By interpolat-

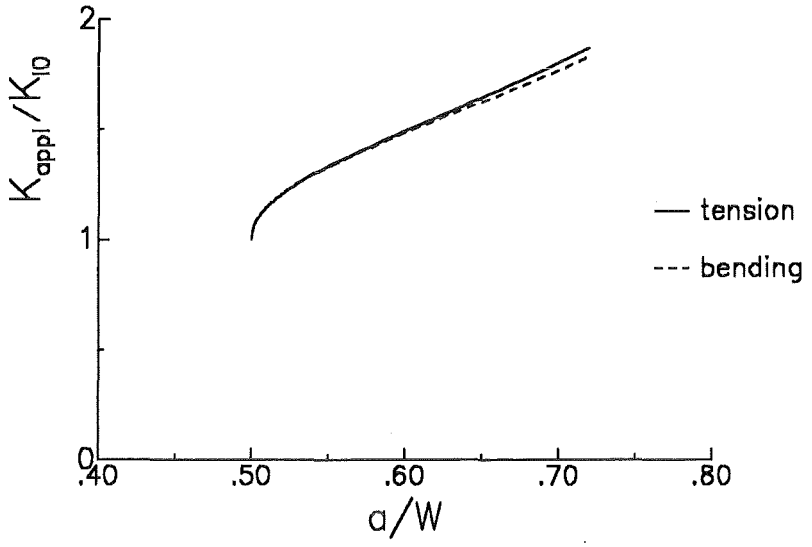

Figure 25. . R-curve for a crack of initial crack depth $a_0/W = 0.5$ computed with eqs.(2.3a) and (2.6) for the bridging stress relation (A1 + A2); Loading cases: bending (dashed curve), tension (solid curve).

ing the computed points $\sigma_{appl} = f(\delta')$ for the considered discrete crack lengths, the curve of fig.28 results.

The real potential energy which leads to the energy release rate is illustrated in fig.28 as hatched area. The energy release rate resulting from fig.28 is plotted in fig.29. Within the error band of numerical computations we can conclude that - in agreement with eq.(3.26) - the energy release rate is constant and the related stress intensity factor equals K_{I0}.

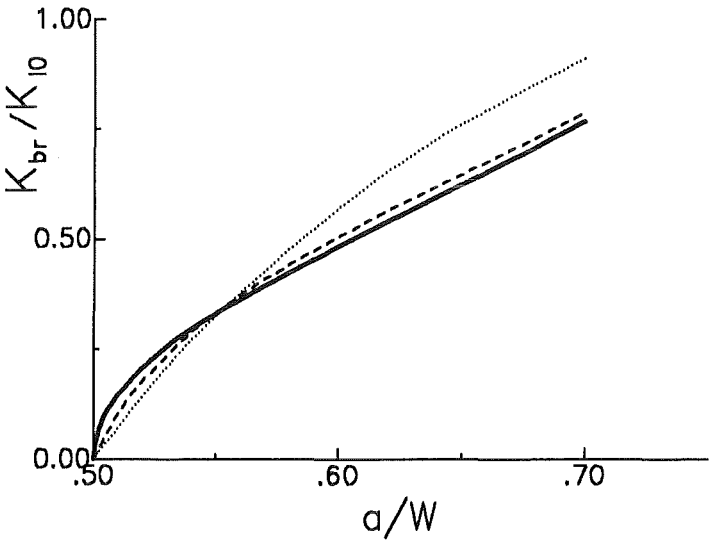

Figure 26. . Comparison of the R-curves ($K_{Ibr} = f(\Delta a)$ for different bridging stress relations; solid line: (A1 + A2), dashed line: (A1 + A5), dotted line: (A11).

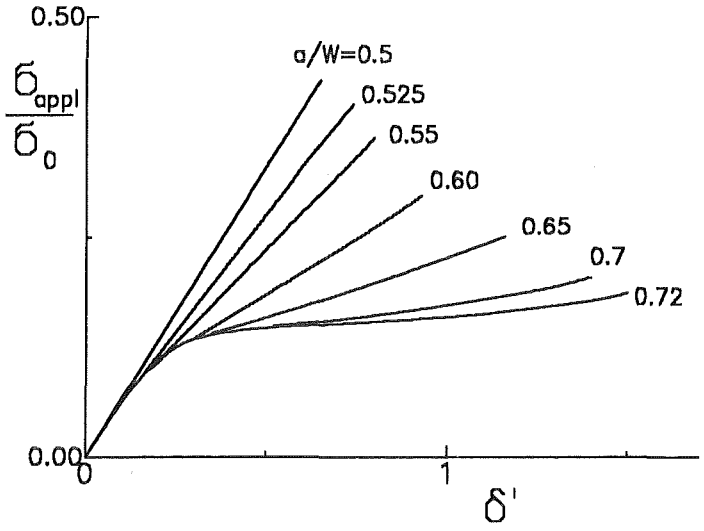

Figure 27. . Load-displacement curves for a crack with bridging interactions according to eqs.(A1 + A5), $a_0/W = 0.5$ (loading: pure tension), abscissa δ' normalised according to eq.(4.5).

- If we ignore completely the non-linear load-displacement behaviour, we may interpret the hatched area in fig.30 as the change of potential energy ΔU_p.
  The elastic energy and its increment are

$$W_{el} = \frac{1}{2} P \delta_{LP} \quad \Rightarrow \quad dW_{el} = \frac{1}{2} (P\, d\delta_{LP} + \delta_{LP}\, dP) \tag{4.12}$$

and the work of the external force is

$$dA = P\, d\delta_{LP} \tag{4.13}$$

The change of the potential energy is

$$dU_p = dA - dW = \frac{1}{2} \left(P\, d\delta_{LP} - \frac{\delta_{LP}}{P^2}\, dP \right) \tag{4.14}$$

Indroducing the global compliance $C = \delta_{LP}/P$ it results

$$dC = \frac{1}{P} d\delta_{LP} - \frac{\delta_{LP}}{P^2}\, dP \tag{4.15}$$

and eq.(4.14) can be rewritten as

$$dU_p = \frac{P^2}{2} dC \tag{4.16}$$

With the apparent crack length a^* the corresponding energy release rate $\hat{G}$ becomes

$$\hat{G} = \frac{dU_p}{B\, da^*} = \frac{P^2}{2B} \frac{dC}{da^*} \tag{4.17}$$

From the compliance formula eq.(4.2) we find

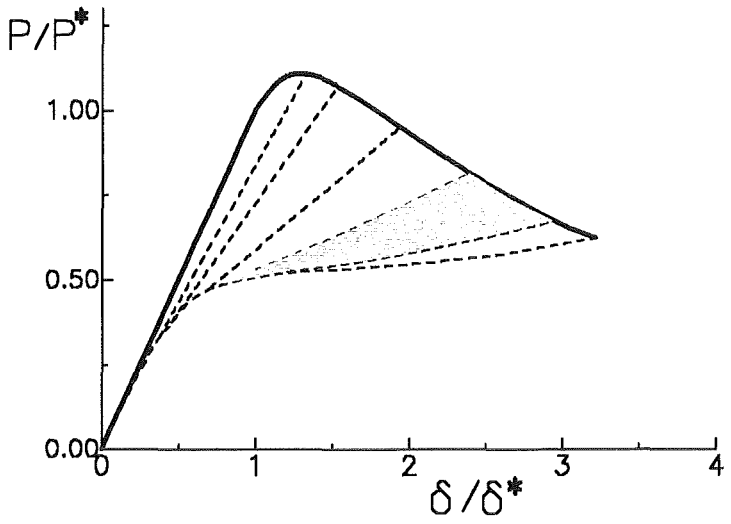

Figure 28. . Load-displacement curve for a controlled fracture test under tension with $K'_{I0}=1$; $a_0/W=0.5$; hatched area: real potential energy dU_p; $\delta^*=$ displacement where $K_{I\,tip}=K_{I0}$ is reached for the first time.

$$\frac{dC}{da^*}=\frac{2}{E'B}Y^2(a^*)\,a^* \tag{4.18}$$

and the apparent stress intensity factor resulting from the Irwin formula

$$\hat{K}_{Iappl}=\sqrt{E'\hat{G}}=\sigma_{appl}\,Y(a^*)\sqrt{a^*} \tag{4.19}$$

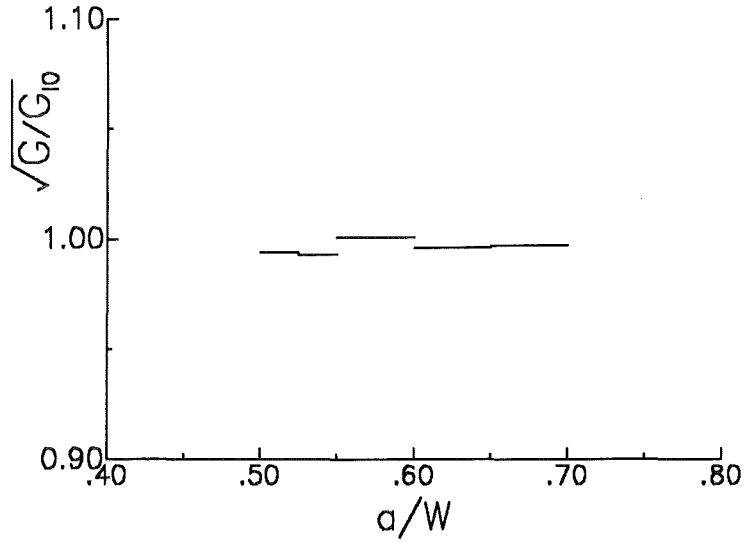

Figure 29. . Averaged energy release rate resulting from the crack increments of fig.28, computed with eq.(3.1).

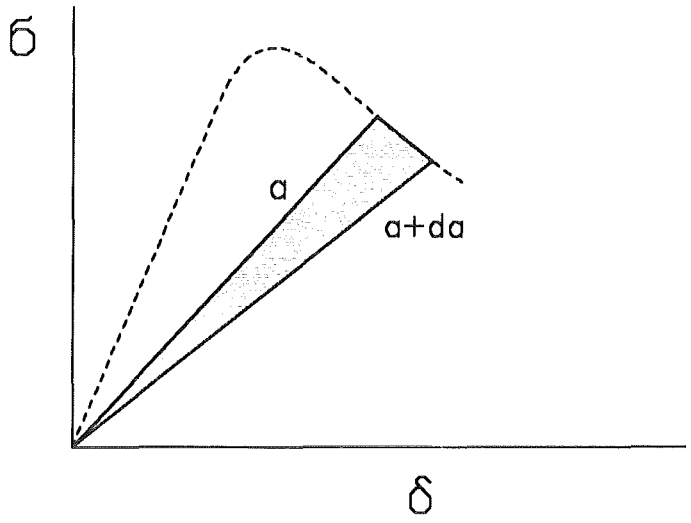

Figure 30. . Increment of apparent potential energy (schematic).

is identical with $\tilde{K}_{Iappl}$ defined by eq.(4.11).

- A second possibility of defining an energy release rate is to use dU_p/da, applying the physical crack depth a. The potential energy can be expressed by

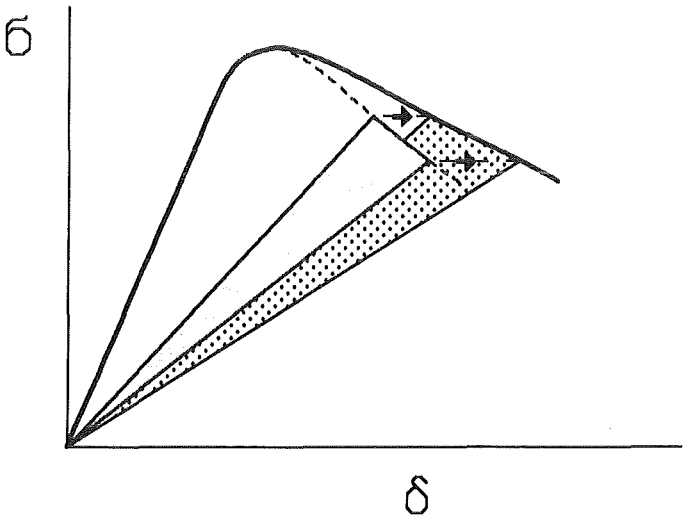

Figure 31. . Increment of apparent potential energy, in case the displacements are shifted until the compliance is in agreement with the compliance of a crack free of bridging interactions (schematic).

$$\bar{G} = \frac{dU_p}{B\,da} = W \int_0^{\sigma_{appl,c}} \left(\frac{\partial \delta'_{LP}}{\partial a} \right)_{\sigma_{appl}} d\sigma'_{appl} \tag{4.20}$$

For the straight lines in fig.30 it holds

$$\frac{\partial \delta'_{LP}}{\partial a} = \frac{\partial \delta_{LP}}{\partial a} \; \frac{\sigma'_{appl}}{\sigma_{appl,c}} \tag{4.21}$$

Evaluation of the integral gives

$$\bar{G} = \frac{dU_p}{Bda} = \frac{W}{2} \sigma_{appl,c} \left(\frac{\partial \delta_{LP,c}}{\partial a} \right)_{\sigma = const} \tag{4.22}$$

and the related stress intensity factor

$$\bar{K}_{appl} = \sqrt{E' \bar{G}} \tag{4.23}$$

Since in the general case $da^*/da < 1$ is fulfilled, one has to expect $\bar{K}_{appl} < \hat{K}_{appl}$.

- The slope of the straight lines in fig.31 defines the apparent crack length. If we shift the displacements at a fixed load (or stress applied) to higher values $\vec{\delta}$ (the arrow symbolises the shifted displacements) until the slope of the new straight line is in agreement with the compliance of the unbridged crack, (fig.31), it holds

$$\vec{\delta}_{LP} = P\,C(a) = \sigma_{appl}\,BW\,C(a) \tag{4.24}$$

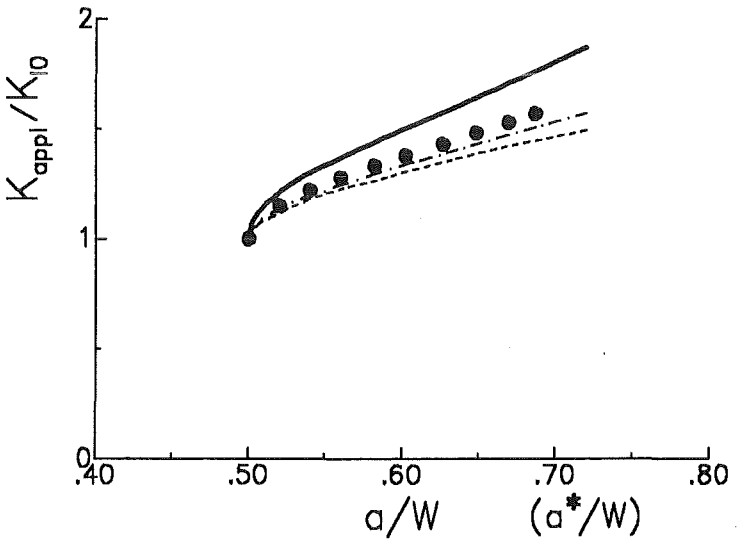

Figure 32. . Comparison of the correct R-curve ($K_{I\,appl}$: solid line) with apparent stress intensity factors resulting from the load-displacement curve: a) $\bar{K}_{appl}$ (dashed curve), b) $\hat{K}_{appl}$ (dash-dotted curve), in addition, the symbols show the apparent stress intensity factor $\hat{K}_{appl}$ plotted versus the apparent crack depth.

The change of the apparent potential energy is

$$\frac{d\vec{U}_p}{da} = BW \int_0^{\sigma_{appl,c}} \left(\frac{\partial \vec{\delta}'_{LP}}{\partial a} \right)_{\sigma = const} d\sigma'_{appl} \tag{4.25}$$

and the straight lines provide

$$\frac{\partial \vec{\delta}'_{LP}}{\partial a} = \left(\frac{\partial \vec{\delta}_{LP}}{\partial a} \right)_{\sigma_{appl,c}} \frac{\sigma'_{appl}}{\sigma_{appl,c}} \tag{4.26}$$

From (4.24) we conclude

$$\left(\frac{\partial \vec{\delta}_{LP}}{\partial a} \right)_{\sigma = const} = BW\, \sigma_{appl,c} \frac{\partial C}{\partial a} \tag{4.27}$$

Introducing (4.26) and (4.27) into (4.24) yields

$$\frac{d\vec{U}_p}{da} = \frac{1}{2} \sigma^2_{appl} \frac{\partial C}{\partial a} \tag{4.28}$$

and with (4.2)

$$\vec{G} = \frac{d\vec{U}_p}{Bda} = \sigma^2_{appl} Y^2(a)\, a \tag{4.29}$$

The related stress intensity factor is

$$\vec{K} = \sqrt{\vec{G}\, E'} = K_{I\,appl} \tag{4.30}$$

It is found to be identical with the applied stress intensity factor $K_{I\,appl}$ computed directly from the crack length and load without consideration of the energy.

Finally, the following relation between the differently defined stress intensity factors holds:

$$\bar{K}_{appl} (<) \hat{K}_{appl} = \tilde{K}_{appl} < \vec{K}_{appl} = K_{I\,appl} \tag{4.31}$$

Figure 32 gives a comparison of these stress intensity factors.

5.0 References

[1] J. R. Rice, Int. J. Solids Structures **8**(1972)751-758
[2] H. Bückner, ZAMM **50**(1970)751.
[3] T. Fett, C. Mattheck, D. Munz, Engng. Fract. Mech. **27** (1987)697-715.
[4] P.C. Paris, Document D2-2195, The Boeing Company, 1957.
[5] H. Tada, "The stress analysis of cracks handbook", Del Research Corporation (1986).
[6] B.N. Cox, D.B. Marshall, Acta metall. **39**(1991)579.
[7] D. Broek, Elementary Engineering Fracture Mechanics, Martinus Nijhoff Publishers, 1986, Dordrecht.
[8] T. Fett, D. Munz, Evaluation of R-curve effects in ceramics caused by bridging interactions, KfK-Report 4940, Kernforschungszentrum Karlsruhe, 1991.
[9] A.G. Evans, R.M. McMeeking, On the toughening of ceramics by strong reinforcements, Acta metall. **34**(1986)2435-2441.
[10] H.G. Hahn, Bruchmechanik, B.G. Teubner, Stuttgart1976.
[11] T. Fett, Influence of bridging stresses on specimen compliances, J. Mater. Sci. Letters **10**(1991),1211-1216.
[12] T. Fett, D. Munz, Influence of crack-surface interactions on stress intensity factor in ceramics, J. Mater. Sci. Letters **9**(1990),1403-1406.
[13] T. Fett, M. Caspers, D. Munz, H. Stamm, Int. J. Fract. **43**(1990),195-211.
[14] T. Fett, "Stress intensity factors and weight functions for the edge cracked plate calculated by the Boundary Collocation Method", KfK-Report 4791, Kernforschungszentrum Karlsruhe, 1990.

Appendix A.

A.1 Bridging relations for numerical calculations

A.1.1 Bridging stresses based on friction effects

In order to provide realistic illustrations, special types of bridging relation are used. For friction-like bridging stresses in the wake of the propagating crack we use

$$\sigma_{br} = \sigma_0 \exp(-\delta/\delta_0)\, g(\delta/\delta_0) \tag{A.1}$$

where $g(\delta/\delta_0)$ is a "switch-on" function for the bridging stresses which avoids that maximum stresses occur in the absence of any displacement. Normally, the authors use a step function

$$g(\delta/\delta_0) = \begin{cases} 0 & \text{for} \quad \delta = 0 \\ 1 & \text{for} \quad \delta > 0 \end{cases} \tag{A.2}$$

The maximum bridging stress occurs at $\delta/\delta_0 = 0$:

$$\sigma_{max} = \sigma_0 \tag{A.3}$$

and the specific work necessary for dissolving the bridges is given as

$$W_{br} = \int_0^\infty \sigma_{br}(\delta)\, d\delta = \sigma_0\, \delta_0 \tag{A.4}$$

In this paper a continuous switch-on function is chosen

$$g(\delta/\delta_0) = 1 - \exp(-20\delta/\delta_0) \tag{A.5}$$

This relation is illustrated in fig.A1. The maximum bridging stresses are found for $\delta/\delta_0 = 0.1522$

$$\sigma_{max} = 0.8179\, \sigma_0 \tag{A.6}$$

and it results

$$W_{br} = \int_0^\infty \sigma_{br}(\delta)\, d\delta = \frac{20}{21}\, \sigma_0\, \delta_0 \tag{A.7}$$

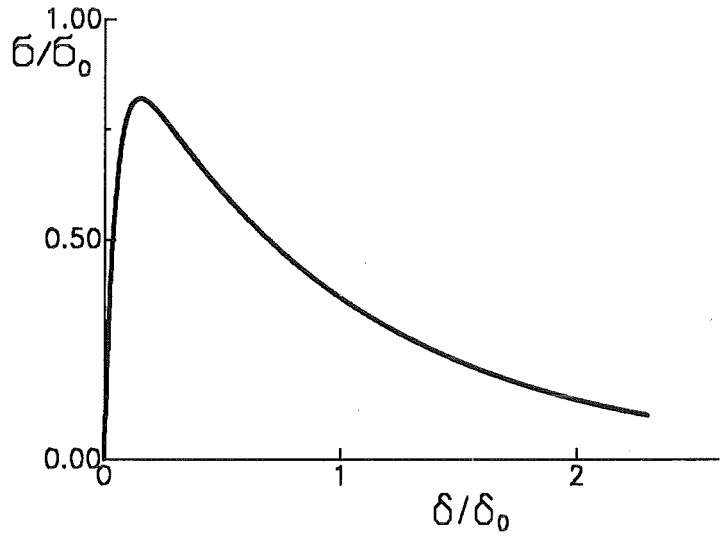

Fig.A1 Stress-displacement relations for friction-like crack surface interactions.

A.1.2 Springs with limited extensions

In case of spring-like stresses the bridging stresses in a single bridge may be expressed by

$$\sigma_{br,spring} = \left\{ \begin{array}{ll} \sigma_0 \delta/\delta_0 & \text{for } \delta/\delta_0 < 1 \\ 0 & \text{for } \delta/\delta_0 > 1 \end{array} \right\} \tag{A.8}$$

with maximum extension δ_0 and maximum stress σ_0, as shown in fig.A2.
Similar to [8], it is assumed that the characteristic displacement δ_0 for which the bridging stresses vanish is Γ-distributed

$$f(\delta_0) = \frac{1}{\delta_{00}} \frac{\delta_0}{\delta_{00}} \exp(-\delta_0/\delta_{00}) \tag{A.9}$$

with a characteristic displacement value δ_{00} characterising the "width" of the distribution. Figure A3 illustrates eq.(A9). The macroscopically averaged bridging stresses result from

$$\sigma_{br} = \int_0^\infty \sigma_{br,spring} f(\delta_0)\, d\delta_0 \tag{A.10}$$

and we obtain by integration and by replacing δ_{00} by δ_0

$$\sigma_{br} = \sigma_0 \frac{\delta}{\delta_0} \exp(-\delta/\delta_0) \tag{A.11}$$

In this case, one obtains at $\delta/\delta_0 = 1$:

$$\sigma_{max} = \sigma_0/e = 0.3679\, \sigma_0 \tag{A.12}$$

and

$$W_{br} = \int_0^\infty \sigma_{br}(\delta)\, d\delta = \sigma_0\, \delta_0 \qquad (A.13)$$

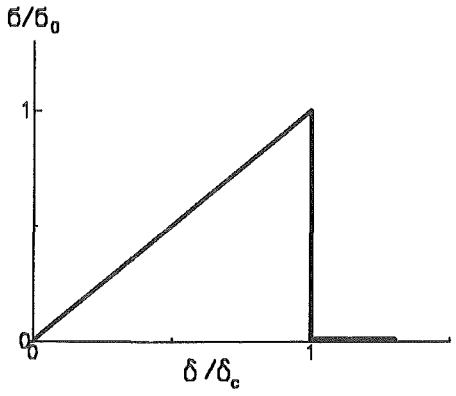

Fig.A2 Stress-displacement relations for a single spring $\sigma_{br}/\sigma_0 = f(\delta/\delta_0)$, eq.(A8).

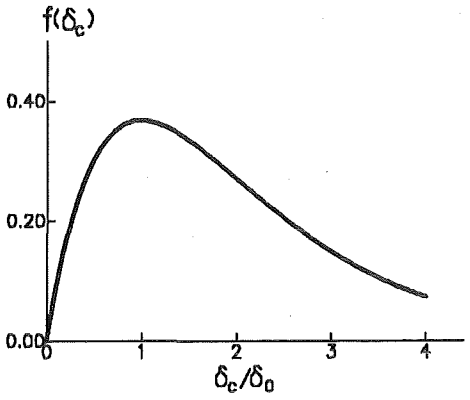

Fig.A3 Distribution of the characteristic COD-value δ_0 (abscissa normalised: δ_0/δ_{00}), eq.(A9).

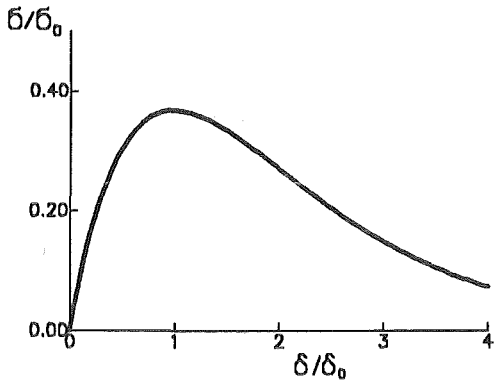

Fig.A4 Stress-displacement relations for spring-like crack-surface interactions.

In [12] the authors used a Morse-like bridging relation

$$\sigma_{br} = \sigma_0[\, \exp(-\delta/\delta_0) - \exp(-2\delta/\delta_0)] \qquad (A.14)$$

with a maximum bridging stress at $\delta/\delta_0 = \ln(2)$:

$$\sigma_{max} = \frac{1}{4}\, \sigma_0 \qquad (A.15)$$

and

$$W_{br} = \int_0^\infty \sigma_{br}(\delta)\, d\delta = \frac{1}{2}\, \sigma_0\, \delta_0 \qquad (A.16)$$

Equation (A.14) together with eq.(A.11) is plotted in fig.A4 in a normalised representation. The agreement is found to be quite good. From this point of view both relations are appropriate to describe spring-like bridging interactions.

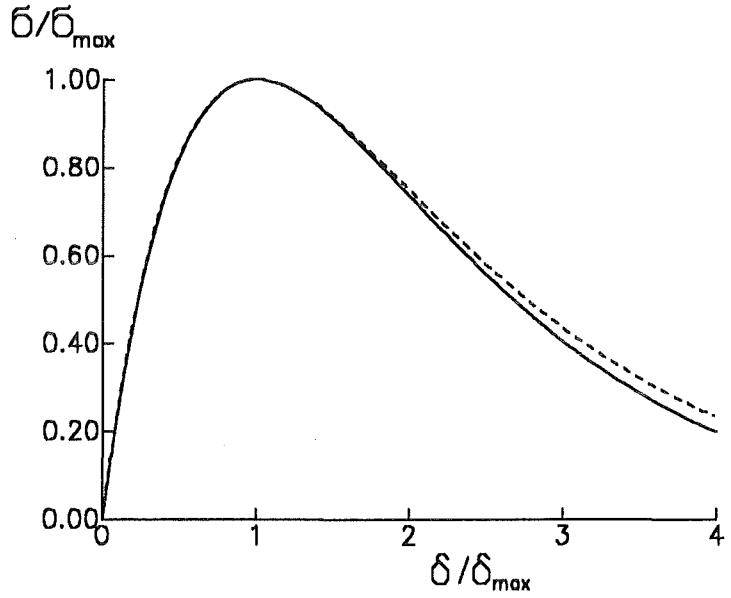

Fig.A5 Comparison of stress-displacement relations; solid curve: eq.(A.11); dashed curve: eq.(A.13).

If we now assume a narrower distribution of the δ_0-values, we can use the next higher order Γ-distribution, namely

$$f(\delta_0) = \frac{1}{\delta_{00}} \left(\frac{\delta_0}{\delta_{00}} \right)^2 \exp(-\delta_0/\delta_{00}) \qquad (A.17)$$

We obtain for the bridging relation

$$\sigma_{br}/\sigma_0 = \frac{\delta}{\delta_0} \left(1 + \frac{\delta}{\delta_0} \right) \exp(-\delta/\delta_0) \qquad (A.18)$$

A comparison between the bridging relations for the first and second order Γ-distributions is given in fig.A6.

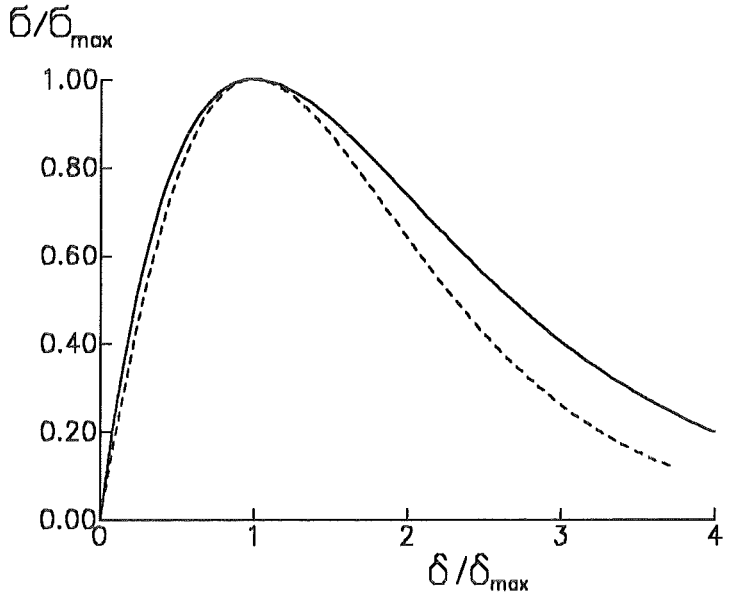

Fig.A6 Comparison of stress-displacement relations; solid curve: eq.(A.7); dashed curve: eq.(A.10).

A.2 Derivation of eq.(2.2)

The weight function formula given by Rice [1] can easily be derived as shown in [13]. The energy release rate for a crack of length a under load σ_1 and crack opening δ_1 is

$$K^2{}_1/E' = G_1 = \frac{\partial}{\partial a}\int_0^a \sigma_1(x)\,\delta_1(x)\,dx \tag{A.19}$$

In a second state of loading, indicated by subscript "2", an equivalent relation holds

$$K^2{}_2/E' = G_2 = \frac{\partial}{\partial a}\int_0^a \sigma_2(x)\,\delta_2(x)\,dx \tag{A.20}$$

Now we superimpose both loadings having in mind that the stress intensity factors have to be simply added. This yields

$$\begin{aligned}\frac{(K_1+K_2)^2}{E'} &= \frac{\partial}{\partial a}\int_0^a (\sigma_1+\sigma_2)(\delta_1+\delta_2)\,dx \\ &= \frac{\partial}{\partial a}\left[\int \sigma_1\,\delta_1\,dx + \int \sigma_2\,\delta_2\,dx + \int \sigma_2\,\delta_1\,dx + \int \sigma_1\,\delta_2\,dx\right]\end{aligned} \tag{A.21}$$

We introduce Betti's theorem

$$\int \sigma_1\,\delta_2\,dx = \int \sigma_2\,\delta_1\,dx \tag{A.22}$$

and obtain

$$\frac{K_1^2}{E'} + \frac{K_2^2}{E'} + 2\frac{K_1 K_2}{E'} = \int \sigma_1 \, \delta_1 \, dx + \int \sigma_2 \, \delta_2 \, dx + 2\int \sigma_2 \, \delta_1 \, dx \qquad (A.23)$$

and after introducing (A.19) and (A.20) in (A.23) we obtain

$$K_2 = \frac{E'}{K_1} \int_0^a \sigma_2 \frac{\partial \delta_1}{\partial a} \, dx = \int_0^a \sigma_2 h(x,a) \, dx \qquad (A.24)$$

and, consequently, if we interpret the state "2" as the reference state "ref"

$$h(x,a) = \frac{E'}{K_{ref}} \frac{\partial \delta_{ref}}{\partial a} \qquad (A.25)$$

A.3 Derivation of eq.(2.4)

From eq.(2.2) it follows

$$\frac{\partial \delta}{\partial a} = h\left(\frac{x}{a}, \frac{a}{t}\right) \frac{K}{H} \qquad (A.26)$$

Here x is the coordinate where the displacement should be computed. Introducing eq.(2.3) leads to

$$\frac{\partial \delta}{\partial a} = \frac{h\left(\frac{x}{a}, \frac{a}{t}\right)}{H} \int_0^a h\left(\frac{x'}{a}, \frac{a}{t}\right) \sigma(x') dx' \qquad (A.27)$$

x' is the location where the stress σ acts. Integrating over a yields

$$\delta = \frac{1}{H} \int_x^a h\left(\frac{x}{a'}, \frac{a'}{t}\right) \left[\int_0^{a'} h\left(\frac{x'}{a'}, \frac{a'}{t}\right) \sigma(x') dx' \right] da' \qquad (A.28)$$

Since the inner integration is not carried out on x , the outer weight function can be taken into the inner integral which leads to

$$\delta = \frac{1}{H} \int_x^a \left[\int_0^{a'} h\left(\frac{x}{a'}, \frac{a'}{t}\right) h\left(\frac{x'}{a'}, \frac{a'}{t}\right) \sigma(x') dx' \right] da' \qquad (A.29)$$

For the weight functions it holds

$$h(a', x) = 0 \quad \text{for} \quad x > a' \qquad (A.30)$$

$$h(a', x') = 0 \quad \text{for} \quad x' > a' \qquad (A.31)$$

Changing the order of integrations yields

$$\delta(x) = \frac{1}{H}\int_0^a \int_{\max(x,x')}^a h(a',x)\, h(a', x')\sigma(x')da'dx' \qquad (A.32)$$

A.4 Relations for bending load

For 3-point bending (fig.A7) the bending stress is given by

$$\sigma_{bend} = \frac{3}{2}\frac{PL}{BW^2} \qquad (A.33)$$

The quantities P,L are explained in fig.A7. The applied stresses in the absence of the crack are

$$\sigma_{appl}(x) = \sigma_{bend}\left(1 - 2\frac{x}{W}\right) \qquad (A.34)$$

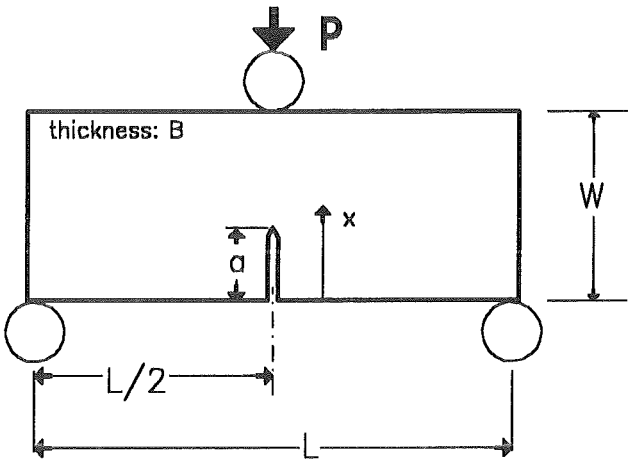

Fig.A7 Three-point bending test.

The increment of work done by the external force P is

$$P\, d\delta_{LP} = 2B\int_0^a \sigma_{bend}\left(1 - 2\frac{x}{W}\right) d\delta_{total}(x)\, dx \qquad (A.35)$$

from which results

$$d\delta_{LP} = \frac{3L}{W^2\sigma_{bend}}\int_0^a \sigma_{bend}\left(1 - 2\frac{x}{W}\right) d\delta_{total}(x)\, dx \qquad (A.36)$$

and, consequently,

$$\frac{\partial \delta_{LP}}{\partial a} = \frac{3L}{W^2 \sigma_{bend}} \int_0^a \sigma_{appl} \frac{\partial \delta_{total}(x)}{\partial a} \, dx \tag{A.37}$$

From (A.36) it results

$$\delta_{LP} = \frac{3L}{W^2} \int_0^a \left(1 - 2\,\frac{x}{W}\right) \delta_{total}(x) \, dx \tag{A.38}$$